
Three finger under-actuated gripper with a break-away clutch mechanism

*A thesis submitted in fulfilment of the requirements
for the degree of Bachelor of Engineering*

by

Kunal Swami (101508062)

Mahesh Chugh (101508066)

Shashwat Jain (101508113)

Harshdeep Lamba (101688009)

Sahil Bhola (101688023)



THAPAR INSTITUTE
OF ENGINEERING & TECHNOLOGY
(Deemed to be University)

Department of Mechanical Engineering

THAPAR INSTITUTE OF ENGINEERING AND TECHNOLOGY

April 2019

Certificate

We hereby declare that the project work entitled "Three finger under-actuated gripper with a break-away clutch mechanism" is an authentic record of our work carried out at Thapar Institute of Engineering and Technology, Patiala as requirements of Capstone project for the award of degree of B.E Mechanical Engineering, Thapar Institute of Engineering and technology, Patiala under the guidance of Prof. S.K. Mohapatra and Asst. Prof. Hema Gurung, during August 2018 to April 2019

April 2019

Certified that the above statement made by the student is correct to the best of our knowledge and beliefs.

Prof. S.K. Mohapatra

Faculty coordinator

Asst. Prof. Hema Gurung

Faculty coordinator

Abstract

Group Number: **G-38**

Degree for which submitted: **B.E.** Department: **Mechanical Engineering**

Thesis title: **Three finger under-actuated gripper with a break-away clutch mechanism**

Thesis supervisor: **Prof. S.K. Mohapatra, Asst. Prof. Hema Gurung**

Month and year of thesis submission: **April 2019**

Today, supply chains are under enormous pressure to keep up with ever-increasing consumer demands. Rapid e-commerce adoption, same-day delivery and omni-channel operations place many new demands on warehouse operations. As a response to this, supply chain executives tend to build bigger warehouses, increase their workforce or add complex technology to achieve gains in productivity. Even with additional investments, the problems cannot always be solved. In the present thesis work, we present the preliminary work on prototype design and analysis of a three-finger under-actuated robotic end effector with a break-away clutch mechanism. The gripper has been modeled and fabricated while simplifying the underlying mechanism and using an off-the-shelf DC servo actuator. The performance of the gripper is evaluated using simulation and experimental data.

Acknowledgements

We are extremely grateful to our thesis supervisor Prof. S.K. Mohapatra and Asst. Prof. Hema Gurung for guidance for our thesis work, which helped us to improve our technical skills. Our supervisors have provided us with opportunities and proper environment to explore the subject. They have been a constant source of inspiration to learn various aspects of Product designing, robotics and research activities. We learned many aspects of mechanical engineering, robotics and CAD/CAE, and further augment our knowledge. We wouldn't have achieved anything without the support and encouragement from our parents. We dedicate this thesis to our teachers, parents, lab-mates and friends.

- G-38

Contents

Certificate	i
Acknowledgements	iii
Contents	iv
List of Figures	vi
List of Tables	ix
1 Introduction	1
1.1 Background	2
1.1.1 Gripper evolution	2
1.1.2 Grip and Rotate	3
1.1.3 Last evolutions	3
1.2 Types of gripper	4
1.2.1 Vacuum gripper	4
1.2.2 Hydraulic gripper	5
1.2.3 Pneumatic gripper	5
1.2.4 Servo-electric gripper	6
1.2.5 Magnetic gripper	6
1.3 Need analysis	6
1.3.1 Augmenting reliability	8
1.3.2 Increase Throughput of the system	9
1.4 Problem statement	11
1.5 Objective	11
2 Methodology	12
2.1 Introduction	12
2.2 Component designing	12
2.2.1 Helical gear designing	12
2.2.2 Spring designing	18

2.2.3	FEA Results	22
2.2.4	Motor selection	31
2.2.4.1	Types of Motor	31
2.2.4.2	Selection criteria	32
2.2.5	Gearhead selection	33
2.2.5.1	Types of Gearhead	33
2.2.5.2	Gearhead selection criteria	34
2.2.6	ADAMS model design	35
2.2.7	Evaluation of grips	36
2.3	Part drawings	40
2.4	Bill of Material	40
3	Fabrication	41
3.1	Introduction	41
3.2	Methodology of Rapid Prototyping	43
3.2.1	Fused Deposition modeling	43
3.2.2	Raw material	45
3.2.3	The FDM 3D Printing Process	46
3.2.4	Accuracy of 3D FDM Printers	47
4	Post-Fabrication analysis	49
4.1	Shrinkage	49
4.1.1	Cause of excessive shrinkage	50
4.1.2	Problems caused by part shrinkage	51
4.2	Warpage	51
5	Conclusion	54
6	Appendix A	56
7	Appendix B	71
8	References	73

List of Figures

1.1	Stanford arm	2
1.2	Suction cups	4
1.3	Hydraulic gripper	5
1.4	Pneumatic gripper	5
1.5	Magnetic gripper	6
1.6	Question 1	7
1.7	Question 2	7
1.8	Question 3	7
1.9	Question 4	8
1.10	Question 5	9
1.11	Question 6	9
1.12	Question 7	10
1.13	Question 8	10
2.1	Gear-pinion assembly	13
2.2	Acting Forces	15
2.3	Material Property	17
2.4	FEA Results	17
2.5	Spring parameters	19
2.6	Element size vs Error	22
2.7	Load case	22
2.8	Results	24
2.9	Steel plate Load case	24
2.10	Results	25
2.11	Results	25
2.12	2D Element quality criteria	26
2.13	3D Element quality criteria	26
2.14	Failure criteria	26
2.15	Gear Load case	27
2.16	Gear Von Misses stress	27
2.17	Gear Displacement	28
2.18	Pinion Load case	28
2.19	Pinion Von Misses stress	28
2.20	Pinion Displacement	29
2.21	Worm wheel Load case	29

2.22 Worm wheel Von Misses stress	30
2.23 Worm wheel Displacement	30
2.24 Spur and Planetary gearhead	33
2.25 Selected motor	35
2.26 Parameters used for contacts	36
2.27 Scematic model of 2 DOF under-actuated finger	37
2.28 Simulation carried out in ADAMS showing grasping sequence	37
2.29 Input Torque characteristics	38
2.30 Contact force on first phalanx while grasping a sphere	38
2.31 Contact force on second phalanx while grasping a sphere	38
2.32 Extension Spring force while grasping the sphere	39
2.33 Spring deformation while grasping the sphere	39
 3.1 difference between the various methods of manufacturing a component	42
3.2 A .stl file being read on simplify 3d	44
3.3 Components fabricated using FDM	44
3.4 Nozzle head of an FDM machine	45
3.5 FDM 3D printing process.	46
3.6 Stratasys uprint an FDM machine.	47
 4.1 The pvT curves for amorphous and crystalline polymers and the specific volume variation (ΔV) between the processing state (point A) and the state at room temperature and atmospheric pressure (point B). Note that the specific volume decreases as the pressure increases.	50
4.2 Processing and design parameters that affect part shrinkage.	50
4.3 Differential shrinkage for both unfilled and filled materials.	52
4.4 Part warpage due to (a) non-uniform cooling in the part, and (b) asymmetric cooling across the part thickness..	52
4.5 Larger volumetric shrinkage due to the high crystallization level in the slow cooling areas (e.g., the thick sections) leads to differential shrinkage and thus part warpage.	53
4.6 The poor cooling of the mold wall on the ribbed side causes a slower cooling of the material on that one side, which can lead to part warpage.	53
 6.1 Lower link	57
6.2 Finger body	58
6.3 Intermediate link	59
6.4 Finger tip	60
6.5 Shaft 40.5	61
6.6 Shaft 10.5	62
6.7 Shaft 14.5	63
6.8 Shaft 26.5	64
6.9 Palm	65
6.10 Helical gear	66
6.11 Worm	67

6.12	Helical gear	24	68
6.13	Pillar	69
6.14	Base	70
7.1	Bill of Material	72

List of Tables

2.1	Motor specification.	34
2.2	Gearhead specification.	34

Chapter 1

Introduction

Robot grippers are attached at the end of an industrial robot. Those are connected as end effector to realize and develop a task in an industrial work floor. They are normally designed as jaws for grasping objects and to move them. The grippers are mostly constructed for opening and closing the jaw. But the evolution of the technology provides the opportunity to bring the grippers to a next level. Such end-effector designs are a micro gripper with piezo-actuator for handling very small objects with complex or flexible shapes, an intelligent robotic gripper for accurate electronic connector mating, a combined gripper with a cutting tool for sweet pepper harvesting, a three-finger pneumatically actuated gripper and an adaptive three-finger robot gripper for use in unstructured industrial application. A lot of end effector designs utilize individual actuation of each joint of the fingers with small high precision DC servo motors. This ensures a high number of controllable degrees of freedom (DOF) suitable for grasping of complex shape objects. However, the presence of multiple actuators in each finger mechanism results in high cost and control complexity of the end effector. A number of designs utilize pulley/tendon actuation mechanisms that are used for industrial and service robotic systems. These mechanisms have advantages in terms of cost due to less number of actuators, have high degree of adaptability and are suitable for different applications. However, these designs have limitations in load carrying capacity and wear resistance. Tendon excursion must be taken into account during the design process. As an alternative there are many studies reported in literature on different designs of under-actuated artificial fingers based on mechanical linkage systems. Above mentioned end-effectors with mechanical linkage system are complex in their manufacturing and have high number of miniature parts. Thus, there is a need for an end effector, providing configurability for different range of grip-ping operations with high

degree of wear and shock resistance, relatively high payload, simple control systems, and simple mechanical structure.

1.1 Background

The first steps of the grippers started in 1969 at the Stanford University by the hand of Victor Scheinman. This mechanical engineer developed the Stanford arm with the first readily controllable gripper. His predecessors, Hydraulic Stanford arm was faster and more effective, but dangerous and uncontrollable. In contrast, Stanford arm was steerable in six full degrees of freedom; gears, harmonic drives and DC motors generated its motion.

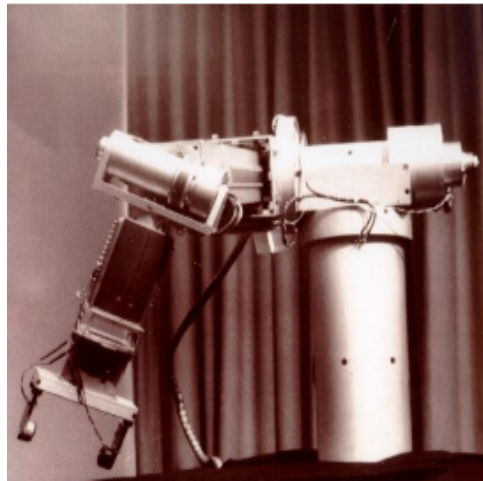


FIGURE 1.1: Stanford arm

In the decade of 1980s more powerful microchips permitted designing rougher grippers based on the Stanford arm for using them in the heavy industry. Even if some feedback and control elements were copied from the Stanford arm the industrial arms started to introduce arms powered by air and used in automotive manufacturing. Nowadays the majority of grippers are still pneumatic.

1.1.1 Gripper evolution

The Stanford arm included a parallel gripper. This configuration is still common nowadays, consisting of two straight fingers (bars) that slide apart or move together to release and grip objects. This is thanks to their stroke versatility. In the late 1970s a two

fingered angle gripper was invented. The fingers are designed for closing like a lobster claw on targeting objects. The difference between these and the parallel fingers is that parallel jaw simplifying the design, and the force stays the same in whole stroke. Parallel fingers have two design options: Direct-acting piston and wedge that give a high grip force (to 44482.22N) and shorter stroke. The other option is straight direct piston which has less force but generates a longer stroke (to 24 in.). A new gripper innovation was invented in the 1980s. A three fingers gripper, designed at the Massachusetts Institute of Technology licensed by Barrett Technology. The con-figuration, Barrett hand, build with servo controllers, communication, four brushless motors and software. Although the three fingers were created in 80s, they are beginning to be used widely now .

1.1.2 Grip and Rotate

Pneumatic powered grippers with traditional cylinders require multiple air supplies. For dual motion units that grip and rotate this is certainly true. In other cases, after establish the initial grip, a mechanical retainer holds the object. The Stanford arm design is still giving inspiration here, in the old breakthrough configuration, slide jaws and electro-mechanical brakes held joints in position and prevented collision damages. Schunk Inc. miniaturized rotating grippers. They produce and assemble thiny components. A parallel gripper is combined with Schunk RM rotary module, which can be equipped with different gripping forces and safety devices for designing semiconductors. Combining rotation with griping requires some modifications. The design adds longer pistons rods for the grip drivers to operate on rotary modules. In addition, finger grippers use a third mounting option in Cartesian gantries as set up. For an easier construction, Schunk's rotator have standardized patterns to adapt and connect plates.

1.1.3 Last evolutions

Till nowadays, robot grippers have been restricted to two and three fingers. But in today's companies as Fest Corp are introducing new technologies combining mechatronics and bionics, more than 30 pneumatic muscles, metacarpal and finger bones, radius and ulna polyamide sintered by laser. Using compressed air with this elastic tubes variates the diameters and length and making them able to develop tasks. An advantage from the human is that muscles don't need energy supply after moving or holding weight in a place. Tensile and contraction forces are monetarized by length and pressure sensors. A regulator distributes pressure in the model giving force, refinement and rapidity. Other ideas are

being developed, such as robotic hands with dexterity and strength of a human one. New microcontrollers bring the possibility of new complex hands with more actuators and adding more strength to the fingers, which makes it possible to create new configurations which are more flexible and efficient for a widely sort of tasks.

1.2 Types of gripper

The End-of -arm has to be in contact with the objects and interact with them. Adapting these ones to the different objects and industrial activities ended with different kinds of grippers. There are four main types of robot grippers: vacuum grippers, hydraulic grippers, pneumatic grippers and servo-electric grippers.

1.2.1 Vacuum gripper

The vacuum gripper has been a standard tool for robots in manufacturing due to its high level of flexibility. The tool is made of polyurethane or rubber suction cup to catch the objects. There are some vacuum grippers that use closed-cells foam rubber layer, in stead of the suction cups.



FIGURE 1.2: Suction cups

1.2.2 Hydraulic gripper

Hydraulic Grippers are the ones that can apply the most strength and often are used in applications that require a huge amount of force. The force is provided from pumps that can generate up to 13789.51 kPa . Although their strength, they are messier than any other gripper due to the oil that the pumps are using. Also they need more maintenance because of the huge amount of force that they can apply.

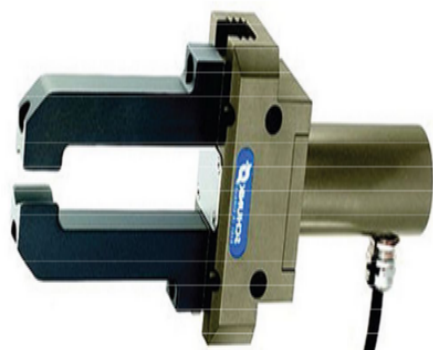


FIGURE 1.3: Hydraulic gripper

1.2.3 Pneumatic gripper

Pneumatic grippers are popular due to their light weight and compact size. They can be design for tight spaces, which can be helpful in manufacturing industry. This kind of gripper can be open and close; because of this their nickname is “bang bang” actuators, given by the sound they do when the metal-on -metal is operating.



FIGURE 1.4: Pneumatic gripper

1.2.4 Servo-electric gripper

The servo-electric grippers are becoming more used in the industry; thanks to their easy control. The gripper jaw movements are controlled by electronic motors. These grippers are highly flexible and good for handling different material tolerances. Also they are cost effective because they don't have air lines and are clean.

1.2.5 Magnetic gripper

Magnetic grippers can be configured by permanent magnets or electromagnets. Permanent magnets, don't need of an external supply for grasping , once an object is grasped there is an additional device called stripper push which separate the object from the gripper. In the other hand, there are the electromagnets, including a controller unit and a DC power which can grasp magnetic objects.



FIGURE 1.5: Magnetic gripper

1.3 Need analysis

The gripper is the part of the robot that physically interacts with the objects and the area around it. A good design can improve the efficacy, improving robot inaccuracy, and gives more flexibility to the robot for developing different tasks. Due to the importance

of the gripper created Causey and Quinn (1998) two guidelines for design robot grippers efficiently. These guidelines focus in increasing the reliability of the system and the other one on increasing the throughput of the system. Although they are two different categories, they are partly overlapped.

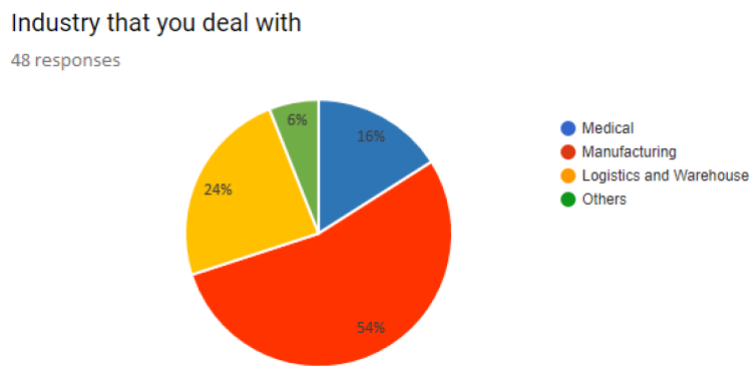


FIGURE 1.6: Question 1

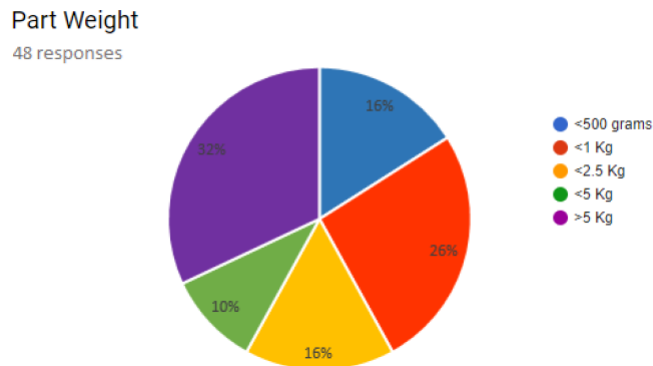


FIGURE 1.7: Question 2

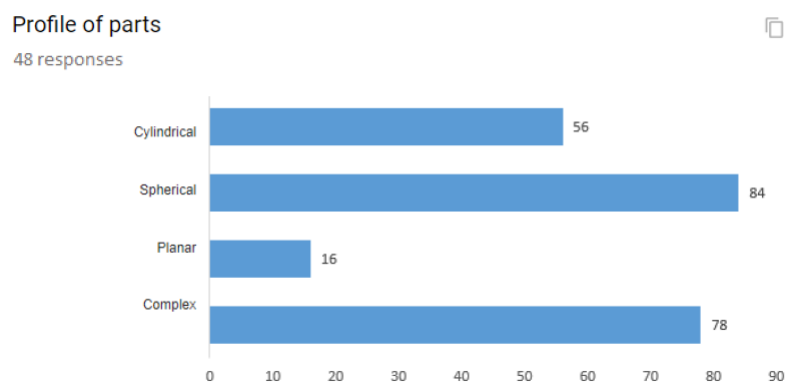


FIGURE 1.8: Question 3

1.3.1 Augmenting reliability

- **Grasp parts Securely:** the part has to be well working for grasping and do not fall or change the position during robot movements.
- **Fully encompass parts with the gripper:** this helps to hold the part securely and align the part in the gripper hand.
- **Chamfer finger's approach surface:** this will decrease the possibility of colliding with the part to grasp.
- **Fingers should align grasped parts:** centre parts on the gripper jaw when this is closed decrease collisions.
- **Proper Gripper-Part interaction:** if the surface of the gripper and the part can align, it improves the grasping reliability
- **Not deform the part during grasping:** If the part is deformed during the process can become useless.
- **Provide and ample approach visualization:** when the system becomes complex a clear vision of the system can simplify the process.
- **Minimize fingers length:** it gives security, because the longer and bigger are the fingers going to be the deflection of this.
- **Incorporate functionality into gripper fingers:** when the gripper grasps an object there is the possibility of error. Designing the fingers to perform extra tasks, because it reduces the chance of release from the gripper.

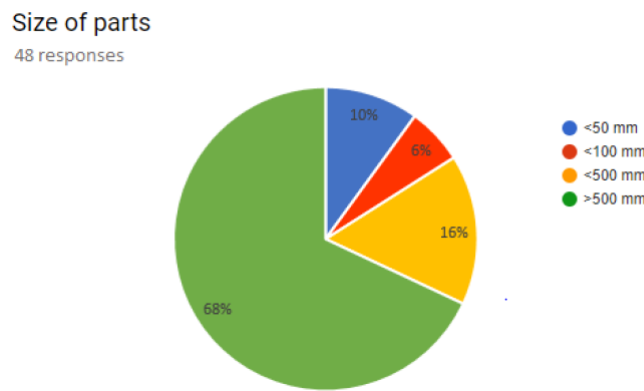


FIGURE 1.9: Question 4

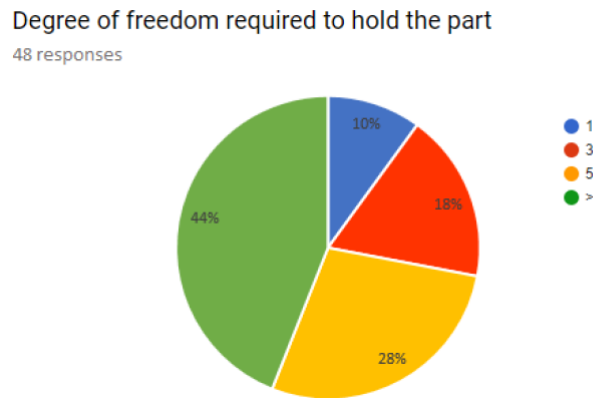


FIGURE 1.10: Question 5

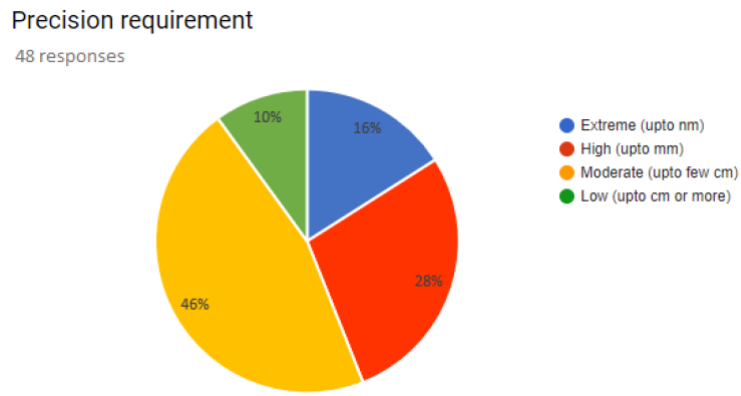


FIGURE 1.11: Question 6

1.3.2 Increase Throughput of the system

- **Minimize gripper footprint:** this is the space that must be free for a successfully grasping.
- **Chamfer gripper fingers' exterior part:** it will displace neighbour parts as the target part wants to be approached.
- **Minimize grippers weight:** this allow the robot to perform better movements and reduce the overshooting.
- **Grasp parts securely:** Secure grasps allows the robot to move at high speed and reduce cycle time.
- **Avoid tool changes:** Changing a gripper needs time and reduce the throughput.
- **Grip multiple parts with a single gripper:** gives more flexibility to a gripper, avoids tool changing and reduces time and cost.

- **Install multiple grippers on a single wrist:** when multiple grippers are ready for using they may decrease the cycle time.
- **Include functionality t in the fingers:** improves the systems flexibility.

In the present work, to study the requirement in the Industry, a market survey was carried out (form attached in Appendix). The results of the survey is shown in Figures 1.6-1.13, which were analyzed to foster a tangible problem statement.

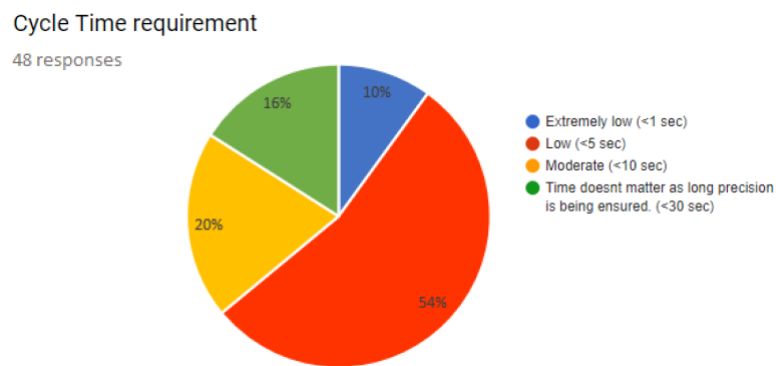


FIGURE 1.12: Question 7

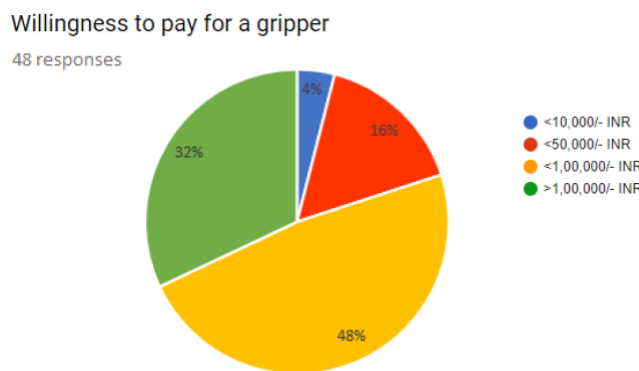


FIGURE 1.13: Question 8

1.4 Problem statement

India's e-commerce market to grow fourfold to 150 billion USD by 2022 with a globally leading annual growth rate of 35%. Recently Amazon in America going a step further to its two day delivery promise announced a one day delivery promise to its 'prime customers'. All this can only be achieved by empowering the lowest rung in the supply chain, the regional warehouses. Expansion of e-retail business with enhanced emphasis on customer satisfaction, inventory of localized content, building digital trust has opened up new avenues of infrastructure development for small scale warehouses that have to be in line with the latest technological developments of supply chain management and industrial automation. The requirements of a warehouse can be summarized as,

- Round the clock accessibility to products in inventory
- Low cost of operations
- Optimal use of storage capacity across its length, breadth and height

A dexterous gripper, fabricated at low costs and requiring low maintenance is a suitable alternative to the unskilled labor currently being employed to shift the packages from shelf to shelf. The existing grippers available in the market are far too ahead in terms of their technological soundness, but industries like these do not require such precise and gentle movements (unless the product is labeled fragile), operating with a small payload (average payload 25N) at the price tag that comes with it (a quick market survey tells us that a conventional gripper costs anything between 75,000 to 3,00,000). Which brings us to the problem statement: "To design and fabricate an adaptable gripper with a simple architecture and enhanced payload at a low cost"

1.5 Objective

- Ensure gripper's feasibility and manufacturability while minimizing cost.
- To demonstrate easiness of modification and add adaptability to the gripper mechanism.
- Use of under-actuation within the end-effector, palm and fingers that provides the full enveloping of the object without prior knowledge of its physical properties.

Chapter 2

Methodology

2.1 Introduction

In this chapter, the designing of various critical components have been shown while employing the principle design methodologies and FEA techniques. Dynamic simulation of the proposed mechanism has also been carried out to check the feasibility of the design and post-process the results. Since one of the primary objective remains cost effectiveness, proposed design has been decided which meets that objective. To quantify the product cost, we have included the Bill of material (BOM).

2.2 Component designing

In this section, we have used the basic machine design principles to design the critical components of the robotic gripper assembly.

2.2.1 Helical gear designing

The teeth of helical gears are cut in the form of a helix on the pitch cylinder. In helical gears, the contact between meshing teeth begins with a point on the leading edge of the tooth and gradually extends along the diagonal line across the tooth. There is a gradual pick-up of load by the tooth, resulting in smooth engagement and quiet operation even at high speeds. Parallel helical gears operate on two parallel shafts. In this case the magnitude of the helix angle is the same for the pinion and the gear, however, the hand of

the helix is opposite. A right-hand pinion meshes with a left-hand gear and vice versa.

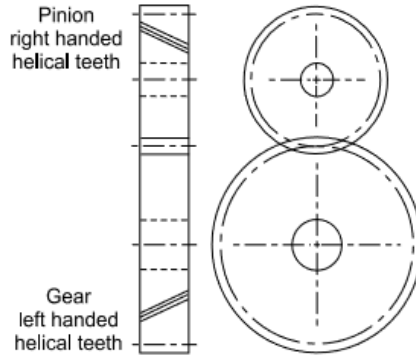


FIGURE 2.1: Gear-pinion assembly

There are two pressure angles, transverse pressure angle (α) and normal pressure angle α_n in their respective planes. It can be proved that they are related by the following expression,

$$\cos \psi = \frac{\tan \alpha_n}{\tan \alpha} \quad (2.1)$$

The normal pressure angle is usually 20° . The pitch circle diameter d of the helical gear is given by,

$$d = \frac{z m_n}{\cos \psi} \quad (2.2)$$

The centre to centre distance a between the two helical gears having z_1 and z_2 as the number of teeth is given by,

$$a = \frac{m_n(z_1 + z_2)}{2 \cos \psi} \quad (2.3)$$

The speed ratio(i) for helical gears is determined in the same manner as for the spur gears, i.e.,

$$i = \frac{\omega_p}{\omega_g} = \frac{z_g}{z_p} \quad (2.4)$$

where suffix "p" and "g" refer to the pinion and gear respectively.

$$18 \text{ teeth for gear} = z_p$$

$$\begin{aligned}
 & 10 \text{ teeth for pinion} = z_g \\
 & i = 1.8 \\
 & \text{module } (m_n) = 2 \\
 & \text{helix angle} = 15 - 25^\circ \text{ (chosen } 20^\circ)
 \end{aligned}$$

Pitch diameter for gears,

$$\begin{aligned}
 d &= \frac{z m_n}{\cos \psi} \\
 \text{gear pitch diameter} &= 38.1 \text{ mm} \\
 \text{pinion pitch diameter} &= 21.1 \text{ mm}
 \end{aligned}$$

Face width of Helical gear,

$$b \geq \frac{\pi m_n}{\sin \psi} \quad (2.5)$$

$$b = 19.18 \text{ mm}$$

Suitable width for manufacturing purpose= 19.25mm, 19.5mm, 20mm

We select, b=20mm

Force Analysis

The resultant force P acting on the tooth of a helical gear is resolved into three components, P_t , P_r and P_a as shown

- P_t = tangential component (N)
- P_r = radial component (N)
- P_a = axial or thrust component (N)

The normal pressure angle α_n is in the plane ABC shaded by dots, while helix angle ψ is in the lower plane BCD.

$$P_r = P_t \left[\frac{\tan \alpha_n}{\cos \psi} \right] \quad (2.6)$$

The tangential component is calculated from the relationship

$$P_t = \frac{2M_t}{d} \quad (2.7)$$

In examples of gear tooth forces, it is often required to find out the magnitude and direction of the three components. The magnitudes are determined by using the following four equations,

$$M_t = \frac{60 * 10^6 (kW)}{2\pi n_p} \quad (2.8)$$

(2.9)

$$P_t = \frac{2M_t}{d} \quad (2.10)$$

(2.11)

$$P_r = P_t \left[\frac{\tan \alpha_n}{\cos \psi} \right] \quad (2.12)$$

(2.13)

$$P_a = P_t \tan \psi \quad (2.14)$$

where the suffix "p" is used for pinion. The following information is required in order to decide the direction of the three components:

- Which is the driving element? Which is the driven element?
- Is the pinion rotating in clockwise or anticlockwise direction?
- What is the hand of the helix? Is it right handed or left handed?

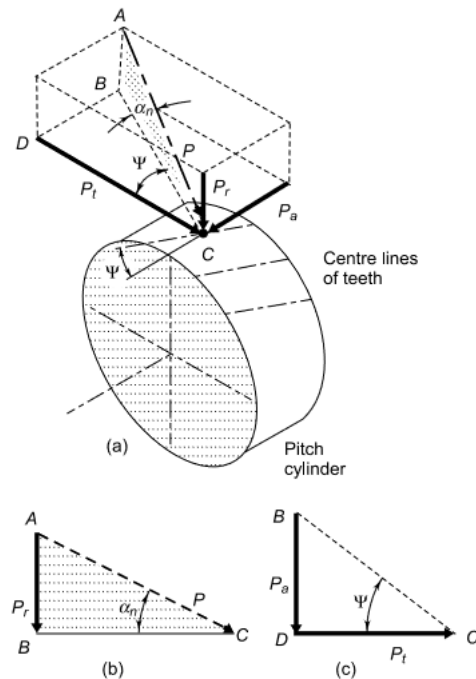


FIGURE 2.2: Acting Forces

The directions of tangential and radial components are decided by the same method that is used for spur gears.

Given:

$$\text{Torque} = \frac{1.5}{3} \text{ Nm (per pinion)} M_t = 0.5 \text{ Nm}$$

Calculated Results :

$$P_t = 43.7 \text{ N}$$

$$P_a = 15.1 \text{ N}$$

$$P_r = 16.8 \text{ N}$$

Beam Strength (Pinion)

In order to determine beam strength, the helical gear is considered to be equivalent to a formative spur gear. The formative gear is an imaginary spur gear in a plane perpendicular to the tooth element. The pitch circle diameter of this gear is d' , the number of teeth is z' and the module m_n , the beam strength of the spur gear is given by

$$S_b = mb\sigma_b Y \quad (2.15)$$

$$S_b = (S_b)_n \cos \psi \quad (2.16)$$

Therefore, beam strength $(S_b)_n$ indicates the maximum value of tangential force that the tooth can transmit without bending failure. It should be always more than the effective force between the meshing teeth.

Effective Load,

$$P_{eff} = \frac{C_s P_t}{C_v} \quad (2.17)$$

where,

C_s = service factor (1.00 from Design Data Book, V.B. Bhandari) C_v = velocity factor
The velocity factor for helical gears is given by

$$C_v = \frac{5.6}{5.6 + \sqrt{v}} \quad (2.18)$$

where, v is the pitch line velocity at 60 RPM= 49.465 mm/sec. Therefore, $C_v = 0.443$.
 $P_{eff} = 98.64N(prelim)$

Material Selection

For 3D printing of the spur gears the available materials are PLA, ABS, Nylon12, PC, the factor of safety for designing of the gears is taken as 2, upon applying the effective load calculated in the previous section and estimating the beam strength of the gears in each case following results were obtained.

Material	Density (g/cc)	Tensile Strength (Mpa)		young's modulus (Gpa)
		yield	ultimate	
PLA	1.29	44.8	50.1	3.76
ABS	1.05	40.7	41.4	2.01
NYL12	1.42	45.4	79.4	5.31
PC	1.2	63.6	60.6	2.36

FIGURE 2.3: Material Property

Sr.no.	Material	weight (kg)	Stress (Mpa)	Deformation (mm)	Tangential Load (N)
1	PLA	0.028	7.67	0.414	133.77
2	ABS	0.022	6.34	0.613	110.53
3	NYL12	0.03	12.16	0.464	211.99
4	PC	0.026	9.28	0.798	161.8

FIGURE 2.4: FEA Results

On the basis of above results and costing of the materials, ABS was chosen as the final material for the fabrication of helical gears.

Material Conformation

Based on the beam strength estimation using dynamic loading. In the final stages of gear design, when gear dimensions are known, errors specified and the quality of gears determined, the dynamic load is calculated by equation derived by Earle Buckingham. The dynamic load is given by,

$$P_d = \frac{2lv(Ceb \cos^2 \psi + P_t) \cos \psi}{2lv + \sqrt{(Ceb \cos^2 \psi + P_t)}} \quad (2.19)$$

where,

P_d = dynamic load or incremental dynamic load (N) = 206.7 N (Upon calculations)

v = pitch line velocity (m/s) = 49.465 mm/sec (from previous section)

C = deformation factor (N/mm^2) = $77000N/mm^2$ (Design data Book)

e = sum of errors between two meshing teeth (mm) = 0.16mm (for Grade 12 3D printing
 $e_p + e_g$)

b = face width of tooth (mm) = 20 mm (from previous section)

P_t = tangential force due to rated torque (N) = 43.7 N (from previous section)

y = helix angle (degrees) = 20 deg (from previous section)

The effective load is given by, $P_{eff} = (C_s P_t + P_d)$

Effective Load=206.7 N

Factor of safety hence calculated = 1.515

Hence the design is safe and fit for production.

2.2.2 Spring designing

The main dimensions of a helical spring subjected to compressive or extensive forces are as follows:

d = wire diameter of spring (mm)

D_i = inside diameter of spring coil (mm)

D_o = outside diameter of spring coil (mm)

D = mean coil diameter (mm)

$$D = \frac{D_i + D_o}{2} \quad (2.20)$$

For the application two springs are to be designed one compressible and one extensive. For the designing of the extensive spring the stiffness of the compression spring must be known hence we proceed as following.

Spring stiffness

Constraints,

Length \downarrow 40mm for both springs Outer Diameter \downarrow 20mm for both springs

The compression force acting on the spring is that of the axial force exerted by the helical gear, hence

$$F_x = F_t \tan \psi$$

We know that $\psi = 20^\circ$ and $F_t = 2T/D$

where T is the torque exerted by the motor, (1.5 Nm). D is the diameter of the helical gear, (38.1 mm).

Therefore, $K_c = F_t/x$. Where, x is the thickness of the helical gear (20 mm).

$$K_c = 1.5 \text{ N/mm}$$

and for the system to work it is important that $K_e < K_c$, therefore we decide $K_e = 1.25 \text{ N/mm}$

Design Procedure

The Indian Standard 4454–1981 has recommended the following value for the permissible shear stress.

$$\tau = 0.5S_{ut}$$

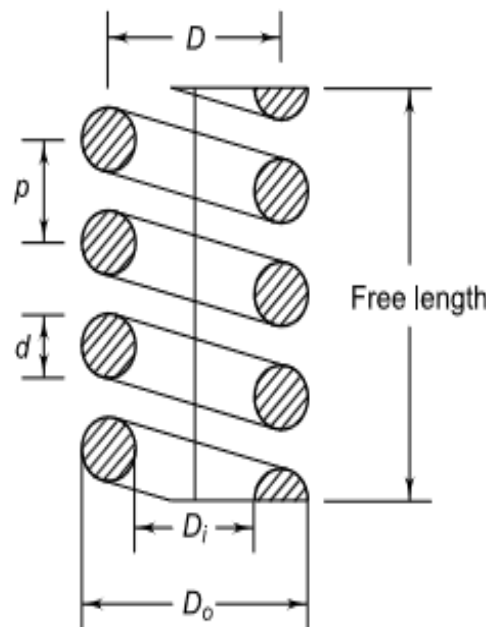


FIGURE 2.5: Spring parameters

The basic procedure for the design of helical spring consists of the following steps:

- For the given application, estimate the spring stiffness (K) and the corresponding required deflection (d) of the spring. In our case $K = 1.5\text{N/mm}$ and $D=20\text{mm}$
- Select a suitable spring material and find out ultimate tensile strength (S_{ut}) from the data. Calculate the permissible shear stress for the spring wire
- Assume a suitable value for the spring index (C). For industrial applications, the spring index varies from 8 to 10. A spring index of 8 is considered as a good value. The spring index for springs in valves and clutches is 5. The spring index should never be less than 3. The spring index chosen for our purpose is 5.
- Calculate the Wahl factor by the following equation:

$$K = \frac{4C - 1}{4C - 4} + \frac{0.615}{C}$$

- Determine wire diameter (d) by

$$\tau = K \left(\frac{8PC}{\pi d^2} \right)$$

- Determine mean coil diameter (D) by the following relationship: $D = c * d$
- Determine the number of active coils (N) by

$$\delta = \frac{8PD^3N}{Gd^4}$$

The modulus of rigidity (G) for steel wires is $81\ 370\ \text{N/mm}^2$.

- Decide the style of ends for the spring depending upon the configuration of the application. Determine the number of inactive coils. Adding active and inactive coils, find out the total number of coils (N_t). For our case, we will be using flat square end and for the extension spring, with number of active coils (N) = $N_t - 2$
- Determine the actual deflection of the spring
- Assume a gap of 0.5 to 2 mm between adjacent coils, when the spring is under the action of maximum load. The total axial gap between coils is given by, Total gap = $(N_t - 1)$ gap between two adjacent coils In some cases, the total axial gap is taken as 15% of the maximum deflection.

- Determine the free length of the spring by the following relationship: free length = solid length + total gap + d
- Determine the rate of spring.
- Prepare a list of spring specification. A helical compression spring that is too long compared to the mean coil diameter, acts as a flexible column and may buckle at a comparatively low axial force. The spring should be preferably designed as buckle-proof. Compression springs, which cannot be designed buckle-proof, must be guided in a sleeve or over an arbor.

Compression Spring design

Upon Calculation, the final values obtained for the compression spring are;

Wire Diameter = 1.5 mm

Outer Diameter = 20 mm

Inner Diameter = 17 mm

End type = Flat Square Ground

Total coils = 7

Free Length = 30 mm

Extension Spring design

Upon Calculation, the final values obtained for the extension spring are;

Wire Diameter = 1.25 mm

Outer Diameter = 15 mm

Inner Diameter = 12.5 mm

End type = Full Hook

Total coils = 7

Free Length = 36 mm

2.2.3 FEA Results

To evaluate the structural strength of the designed components, we have carried out the Finite Element Analysis on the critical components. In this section, we present the results for the carried out analysis.

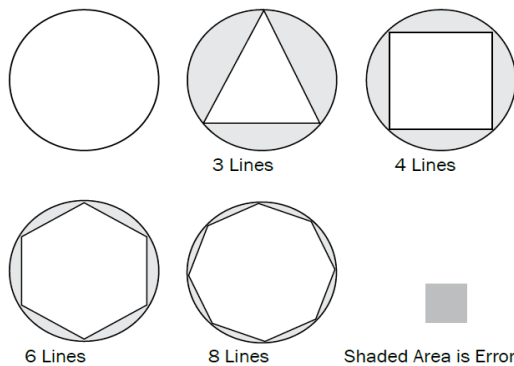


FIGURE 2.6: Element size vs Error

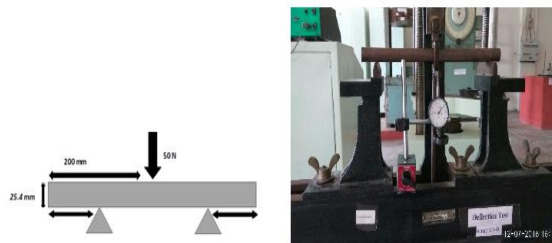


FIGURE 2.7: Load case

Underlying principle

The Finite Element Analysis (FEA) is the simulation of any given physical phenomenon using the numerical technique called Finite Element Method (FEM). Engineers use it to reduce the number of physical prototypes and experiments and optimize components in their design phase to develop better products, faster. It is necessary to use mathematics to comprehensively understand and quantify any physical phenomena such as structural or fluid behavior, thermal transport, wave propagation, the growth of biological cells, etc. Most of these processes are described using Partial Differential Equations (PDEs). However, for a computer to solve these PDEs, numerical techniques have been developed over the last few decades and one of the prominent ones, today, is the Finite Element

Analysis. Differential equations can not only describe processes of nature but also physical phenomena encountered in engineering mechanics. These partial differential equations (PDEs) are complicated equations that need to be solved in order to compute relevant quantities of a structure like stress, strain, etc. in order to estimate a certain behavior of the investigated component under a given load. It is important to know that FEA only gives an approximate solution of the problem and is a numerical approach to get the real result of these partial differential equations. Simplified, FEA is a numerical method used for the prediction of how a part or assembly behaves under given conditions. It is used as the basis for modern simulation software and helps engineers to find weak spots, areas of tension, etc. in their designs. To be able to make simulations, a mesh, consisting of up to millions of small elements that together form the shape of the structure needs to be created. Calculations are made for every single element. Combining the individual results gives us the final result of the structure. Choosing the appropriate element size in order to reduce the computational time and increasing the accuracy is a major trade off.

For choosing the appropriate Element size to be used for meshing of all parts, we performed three analyses on Hypermesh using Optistruct as solver for various sizes of the elements that are as follows:

- **Mild Steel Cylindrical tube** Tube Specifications: Diameter-25.4 mm, thick 2.4mm and 400mm long. The boundary conditions are mentioned below:

The steps followed while performing the Finite Element Analysis on the above described case are:

- **Pre-processing** The Mild steel tube has been meshed using shell elements of different sizes
- **Material** MAT1 card (Defines the material properties for linear, temperature-independent, isotropic materials) was assigned with the properties of AISI 1010
- **Properties** PSHELL card (2D elements), were used and assigned with the thickness of 1mm.
- **Analysis** Linear Static Analysis was performed

Element size of 1 was chosen as the results produce less deflection from the original value and also takes less computational time. The results obtained are shown in Figure 2.8.

- **Steel Plate** Specifications: 200mmx50mmx2mm. The boundary conditions are mentioned here along with the specifications of the Plate. The steps followed while

performing the Finite Element Analysis on the above described case are:

- **Meshing** The Steel Plate has been meshed using shell elements of different sizes
- **Material** MAT1 card (Defines the material properties for linear, temperature-independent, isotropic materials) was assigned with the properties of AISI 1010
- **Properties** PSHELL card (2D elements), were used and assigned with the thickness of 1mm.
- **Analysis** Linear Static Analysis was performed

Element size of 1 was chosen as the results produce less deflection from the original value and also takes less computational time. The results obtained are shown in Figure 2.10.

- **Aluminum Plate** Specifications: 200mmx50mmx2mm. The boundary conditions and plate specifications are same as above. Steps undertaken are as follows

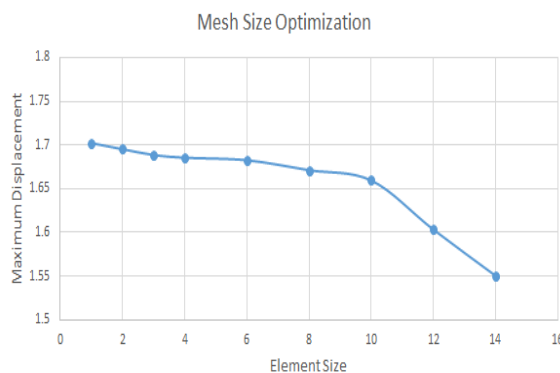


FIGURE 2.8: Results

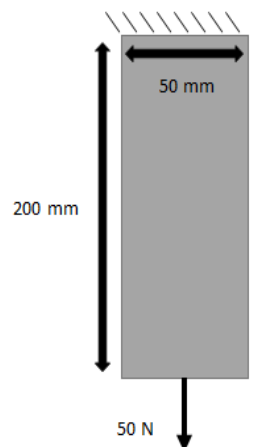


FIGURE 2.9: Steel plate Load case

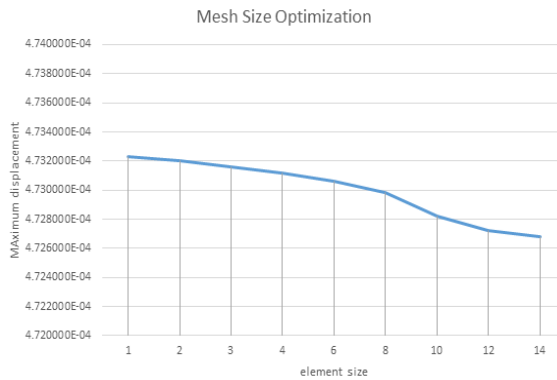


FIGURE 2.10: Results

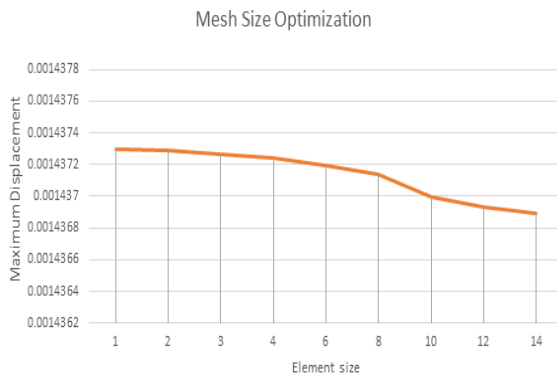


FIGURE 2.11: Results

- **Meshing** The Aluminum Plate has been meshed using shell elements of different sizes
- **Material** MAT1 card (Defines the material properties for linear, temperature-independent, isotropic materials) was assigned with the properties of AISI 1010
- **Properties** PSHELL card (2D elements), were used and assigned with the thickness of 2mm.
- **Analysis** Linear Static Analysis was performed

Element size of 1 was chosen as the results produce less deflection from the original value and also takes less computational time. The results obtained are shown in Figure 2.11.

Quality criteria

Warpage	<	25°
Jacobian	<	0.7
Length	>	3mm
Max % of trias	<	6%
Min quad angle	>	45°
Max quad angle	<	135°
Min tria angle	>	25°
Max tria angle	<	130°

FIGURE 2.12: 2D Element quality criteria

Tetcollapse	<	0.1
-------------	---	-----

FIGURE 2.13: 3D Element quality criteria

While meshing the various components, following quality criteria has been maintained to produce an optimized mesh that will further produce less deviation from the original results, and lead to more accurate results.

- 2D Element quality criteria is shown in Figure 2.12
- 3D Element quality criteria is shown in Figure 2.13

Failure criteria

Maximum Principal stress theory was used as a design Failure criteria.

$$\sigma_{\max} = (\sigma_x + \sigma_y)/2 + \sqrt{[(\sigma_x - \sigma_y)/2]^2 + T_{xy}^2}$$

Where:

σ_{\max} = maximum principal stress

σ_x and σ_y = Normal stresses in X and Y direction

T_{xy} = Shear stress in XY plane

So as per maximum principal stress theory/criterion, the material will be safe if

$$\sigma_{\max} < \sigma_{ut}$$

FIGURE 2.14: Failure criteria

Results

- **Gear** Linear static load simulation was carried out for the gear, with the following load case

- $P_t = 43.7 \text{ N}$
- $P_a = 15.1 \text{ N}$
- $P_r = 16.8 \text{ N}$

The load case is presented in Figure 2.15, followed by the Elemental stress acting on the component in Figure 2.16. It is observed that a maximum stress of 3.18 MPa acts on the component. Elemental displacements is shown in Figure 2.17.

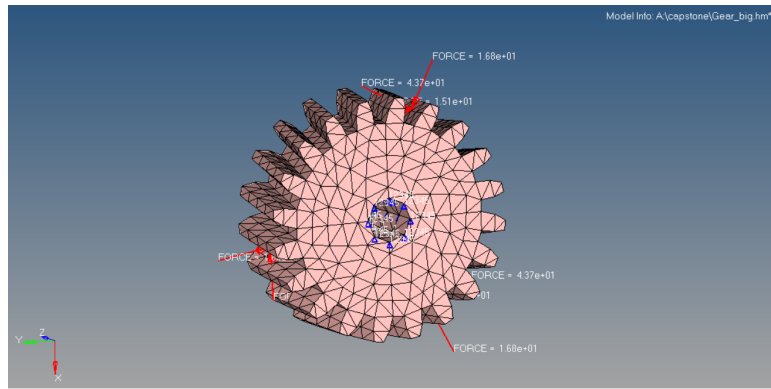


FIGURE 2.15: Gear Load case

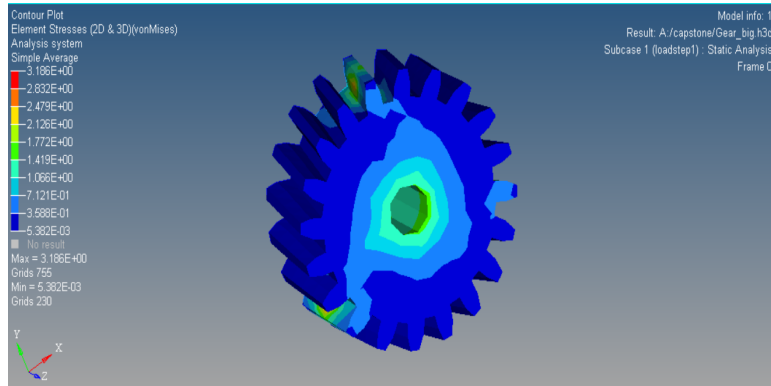


FIGURE 2.16: Gear Von Misses stress

- **Pinion** Linear static load simulation was carried out for the Pinion, with the following load case

- $P_t = 43.7 \text{ N}$

- $P_a = 15.1 \text{ N}$
- $P_r = 16.8 \text{ N}$

The load case is presented in Figure 2.18, followed by the Elemental stress acting on the component in Figure 2.19. It is observed that a maximum stress of 45.2 MPa acts on the component. Elemental displacements is shown in Figure 2.20.

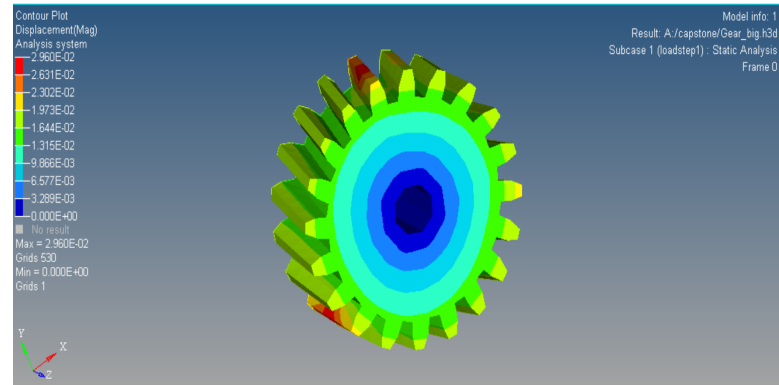


FIGURE 2.17: Gear Displacement

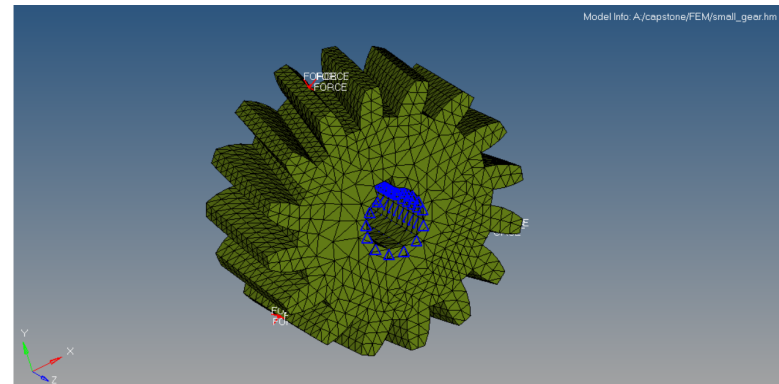


FIGURE 2.18: Pinion Load case

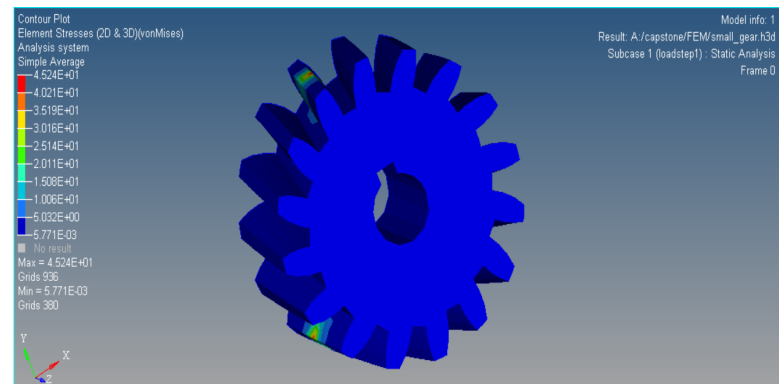


FIGURE 2.19: Pinion Von Misses stress

- **Worm gear** Linear static load simulation was carried out for the worm gear, with the following load case

- Rotation along the axis of the worm gear is allowed (5 DOF constrained)
- Spring force of 9N is acting on the gear face
- $P_r =$ Force of 40N acting at the Helical gear engagement.

The load case is presented in Figure 2.21, followed by the Elemental stress acting on the component in Figure 2.22. It is observed that a maximum stress of 13.9MPa acts on the component. Elemental displacements is shown in Figure 2.23.

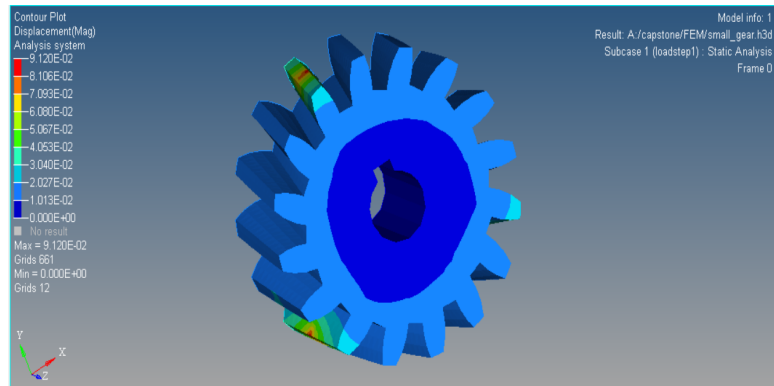


FIGURE 2.20: Pinion Displacement

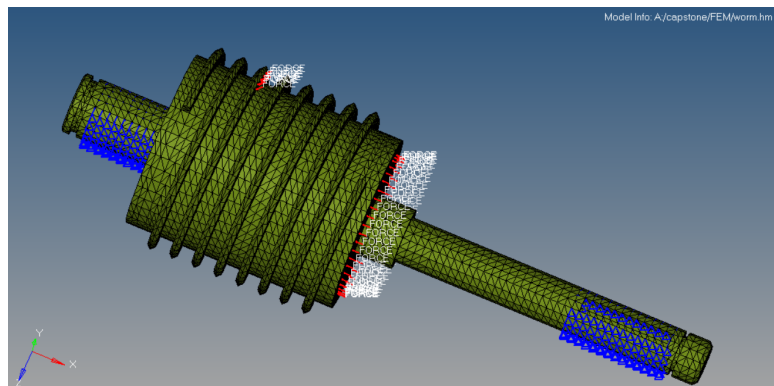


FIGURE 2.21: Worm wheel Load case

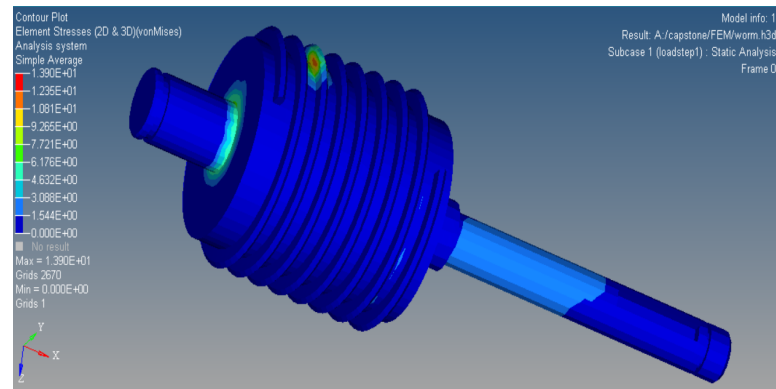


FIGURE 2.22: Worm wheel Von Misses stress

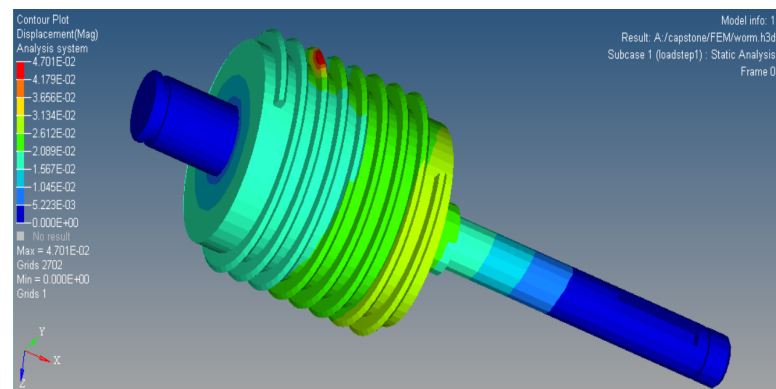


FIGURE 2.23: Worm wheel Displacement

2.2.4 Motor selection

In this section, we will discuss motor selection. First, the available motors will be explained then we will choose the motor based on our requirements.

2.2.4.1 Types of Motor

here are number of electric motors are available in the market, but the brushed DC motor, brushless DC motor and stepper motor are used most commonly in robotic design [1] Some other types of motor are available in the market like induction motor (asynchronous AC motor). [2] The motor that will be discussed are given below:

- **Brushed DC motors** The brushed dc motors are powered by a direct current power source and are internally commutated. They consist of stator and rotor in which stator contains fixed electromagnet or any permanent magnet and other rotor contains an armature with a set of windings. Brushes in this type of motor make mechanical contacts with electrical contacts on the Rotor.
- **Brushless DC motors** With this type of DC motor, a type of synchronous motor, brushes are removed by an external controller element. This means that coils can now be placed inside the stator around the rotor. The advantage is that it improves the heat transport to the outside of the Motor.
- **Stepper motors** The stepper motor is also a type of synchronous motor, which only takes discrete steps. This means that the rotation is divided into a large number of small even steps. The steps taken by stepper motor are smaller than steps taken by a brushless motor and hence give precise control.
- **Induction motors** Induction motor operates on an AC current and it is also called asynchronous motor or AC motor. The working of this motor is that it rotates due to the slip generated by the difference in phase of the rotor and the phase of the stator field. However, the starting torque is low as a result of a non-linearity between the torque and speed. When the motor starts, it draws a large current which results in a voltage drop on the supply line. When light loads are applied to the joint, the power factor decreases significantly, this reduces the efficiency of the motor. [3]
- **Servo motors** They are actuation devices for the precise control of speed, torque, and position. They have better performance and precision when compared to actuation

based on frequency converters, since these do not offer position control and have low effectiveness at low speeds. It contains an encoder which converts the mechanical motion (turns of the shaft) into digital pulses interpreted by a motion controller. It also contains a driver; and in conjunction, they make up a circuit that governs the position, torque, and speed.

So, after taking everything into account we selected DC servo motor because we don't need any complex electronics to run the motor and also offering a unique plug-and-play option to the designer. The servo motor will save the overall cost of the system and as the development costs increase and quantities tend to decrease, it is important to select a DC servo motor.

2.2.4.2 Selection criteria

For selecting the right motor we have used the online Maxon Motor catalog and the following constraints must not be violated.

- **Nominal torque limit** The maximum continues torque is called nominal torque. For this condition, the root mean square (RMS) value of the required motor torque has to be smaller than or equal to the nominal torque of motor i.e. T_m

$$\tau_{rms} \leq T_m$$

where, $\tau_{rms} = \sqrt{\frac{1}{\Delta t} \int_0^{\Delta t} \tau_m^2 dt}$, with Δt being the duration of a working cycle of the motor.

- **Stall torque limit** The peak torque of motor is called stall torque of the motor. The required peak torque has to be smaller than or equal to the stall torque (T_m^{max}) of the motor

$$\tau_p \leq T_m^{max}$$

where $\tau_p = max|\tau_m|$.

- **Maximum permissible speed limit** The commutation system generally limits the maximum permissible speed limit for DC motors. The required peak speed corresponding to the motor has to be smaller than or equal to the maximum permissible

speed (N_m^{max}) of the motor.

$$n_p \leq n_m^{max}$$

The given equations represents the constraints that must not be violated by any motor chosen for operation in any application.

2.2.5 Gearhead selection

In this section we will discuss the gearhead selection. First the available gearhead will be explained. Then we will choose the gearhead based on our requirements.

2.2.5.1 Types of Gearhead

If mechanical power is required at high torque and correspondingly reduced speed, a precision gear is recommended [4]. Motors with built-in gearhead can provide a more cost-effective solution as assembling separate components will require more money. The gear head that will be discussed are Spur and Planetary gearhead.

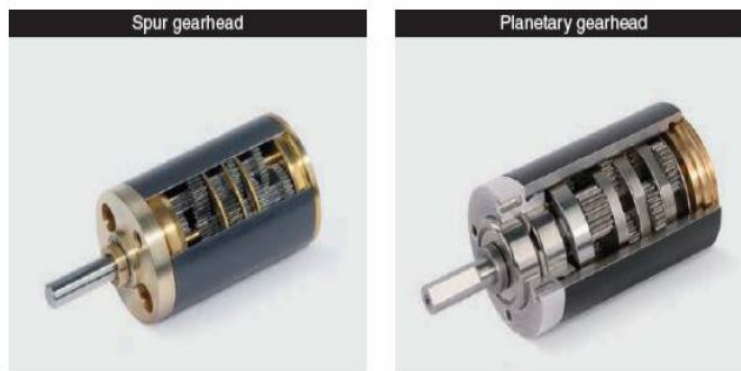


FIGURE 2.24: Spur and Planetary gearhead

Determining the type gear head to be used depends upon the number of factors such as backlash, efficiency, speed, reduction ratio, and cost. Spur gearhead is simple and less expensive but they work for only low-torque applications and planetary gearhead work for a wide range of torque. Torque capacities of spur gearhead are limited because each gear bears the entire load. In planetary gears, the load is distributed over multiple gears i.e. central sun gear is driven by input shaft and it drives the other planet gears. So, by keeping all these things in mind we selected planetary gear head for our application for each and every joint to be driven.

TABLE 2.1: Motor specification.

Index no.	Maxon motor	T_m (mNm)	T_m^{max} (mNm)	N_m^{max} (rpm)	mass (g)
1	DCX16L	1.24	63.3	10700	42

TABLE 2.2: Gearhead specification.

Index no.	Ratio	Maxon gearhead	T_g (Nm)	T_g^{max} (Nm)	N_g^{max} (rpm)	mass (g)
1	186	GPX90	0.86	1.10	14000	43

2.2.5.2 Gearhead selection criteria

Same as the motor selection criteria, in the selection of the gearhead, the following constraints are considered that must not be violated.

- **Maximum output torque limit** The required peak torque τ_g with respect to the output side has to be smaller than or equal to the allowable peak torque T_g^{max} of the gear drive

$$\tau_g \leq T_g^{max}$$

where $\tau_g = \max|\tau_g|$

- **Maximum permissible input speed limit** The required maximum input peak speed n_{in} has to be smaller than or equal to the maximum permissible input speed N_g^{max} of a gearbox

$$n_{in} \leq N_g^{max}$$

The given equations represents the constraints that must not be violated by any gear head chosen for operation in any application. Also, after choosing the gear head we need to convert the speed and torque of the gear output to the motor shaft.

$$n_m = i * n_g$$

$$T_m = \frac{T_g}{i * \eta_g}$$

where, i is the reduction and n_g is the gearhead efficiency. Based upon the equations, motor and gear specifications are calculated and are given in Table 2.1 and Table 2.2 respectively. The selected motor is shown in Figure 2.25.

2.2.6 ADAMS model design

- **Rotational Joints** The revolute joints only have one rotational degree of freedom (D.O.F). which is the same for the torsion springs placed in the same positions. A consequence of using rotational joints between the phalanges is that the model becomes simplified. Since there is only one D.O.F. in each rotational joint – force components acting in other directions than that D.O.F will not affect the finger motion. This in contrast to the physical prototype where these force components would cause friction in the joints which counteract the rotational motions.
- **Mass and Inertia** When the geometries were imported to ADAMS as solids, the model could be assigned mass and inertia by specifying the density of each part. With the density given, ADAMS could calculate the masses and inertias with respect to the volumes of the solids. The density being used was corresponding to the density of the material ABS being used in the prototype with a value of 1070kg/m^3 .
- **Markers** Markers in ADAMS are geometrical points with their own local coordinate system. These markers were given a placing relative to each components local coordinate system. [6] The result of this was that they were given a fix placing in the component which then will follow the component in global moving and this was a necessity to get the force actuation to work as desired.
- **Contact Forces** The ADAMS function Contact Force was used to limit the R.O.M. of the fingers. Between each neighboring finger parts, a Contact Force was defined. This contact force was meant to prevent the phalanges from moving through each other. In other words, the contact forces were defined to make the fingers of the model have the same R.O.M. as the prototype. When defining the Contact Force there are a number of variables to set up, for example, stiffness and penetration depth. The default values of the stiffness and the penetration depth were not satisfying as fluctuations in the contact forces could be seen during what was supposed to be equilibrium. Those values were adjusted until the contact forces became constant in this position when the fingers are fully closed. Two geometries are then selected to

Weight	63g
Stall Torque	12kg.cm at 12V
Positioning Resolution	0.33°
Operation Angle	360° endless turn, electrical position control
Max Speed (no load)	63RPM at 12V
Gear Ratio	194:1

FIGURE 2.25: Selected motor

define which parts the contact force will act between, in this case the object which should be grasped and the finger contact surfaces. The contact damping and stiffness are defined with the relation according to the ADAMS help documentation (REF), where the damping should be set to around of the stiffness for the simulation to run smoothly.

Contact parameters	Value
Static friction coefficient	1.0
Dynamic friction coefficient	0.95
Stiction transition velocity	10 mm/s
Friction transition velocity	2000 mm/s
Contact stiffness	20 N/mm
Force exponent	2,2
Damping	0.001 Ns/mm
Penetration depth	0,01 mm

FIGURE 2.26: Parameters used for contacts

- **Force Actuation of Fingers** The STEP-function is given an initial condition, an end condition, and the timeframe during which the force is varied. The function then returns a value which is calculated with one of the function pieces, in this case the variation of the force is calculated with a cubic polynomial.

2.2.7 Evaluation of grips

One of the main goals of the project was to create a better model than the previous gripper model available in regard to the evaluation of grasp and grasp performances. We have plotted the results of the contact forces generated while grasping the sphere that will be gripped physically. To create the grasp, several versions[7] of the model were created with different objects. Individual contact forces had to be defined for every single surface which was supposed to create contact with the object, and therefore it was better to save the grasps as different files. The contact attributes listed in Table were used to define contact conditions[8] between the object, and the contact patches of the upper and lower phalanx of the fingers.

For motion simulation shown the finger actuation torque is applied to link 1 around pivot point O1 as shown in Figure 2.27 To provide actuation to the second DOF for the finger an extension spring is placed between links 1 and 2. Actuation torque is calculated according

to characteristics[9] of the chosen actuator. All gear ratios are calculated and included in the simulation. Fig. illustrates the simulation results of the finger grasping sequence and the ball shape[10] in the figure represents a grasping object which is fixed to the workspace. The gravity is taken into account[11] and applied in the vertical direction downwards.

The simulation was made with 500 steps with total simulation time was 0.7 seconds. The sphere was grasped by applying the torque of 1.5Nm to the finger and the resultant grip can be seen in the fig. The torque was applied by using the previously described STEP function and the profile can be seen in the fig. Based on the torque profile and mechanism of the finger, the reacting contact forces during the grip were measured with both the contact surfaces and are plotted in the fig. As can be seen, the lower phalanx contact surface generates a maximum force of around 15N as desired for our need and we can see that contact force on upper phalanx is quite low which is expected based on the configuration of the gripper and mechanism used. Also, we have shown the spring forces

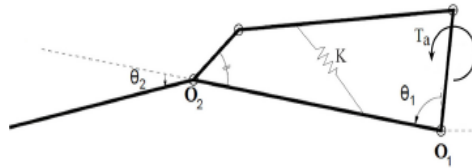


FIGURE 2.27: Scematic model of 2 DOF under-actuated finger

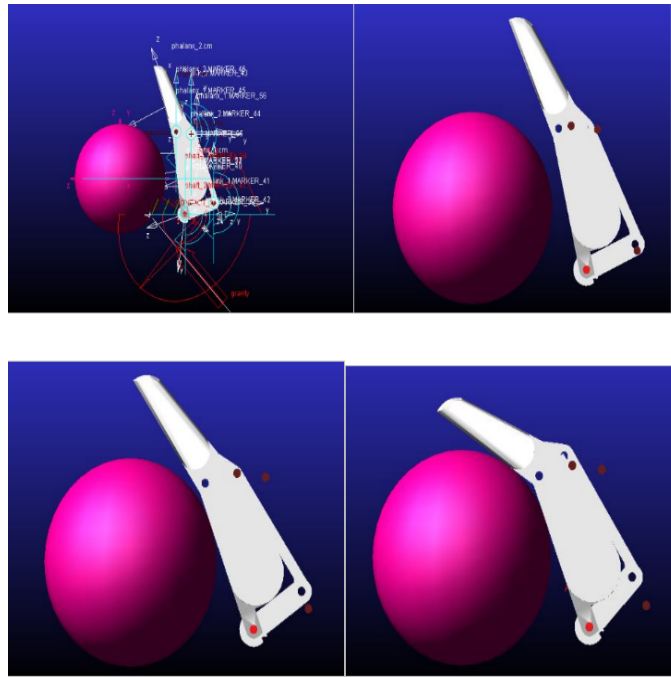


FIGURE 2.28: Simulation carried out in ADAMS showing grasping sequence

and its deflection which occurs due to the grasping sequence[12] performed and it could be seen that the spring forces were of sufficient magnitude[13,14,15] to grasp the sphere with the two phalanx fingers to keep in the place.

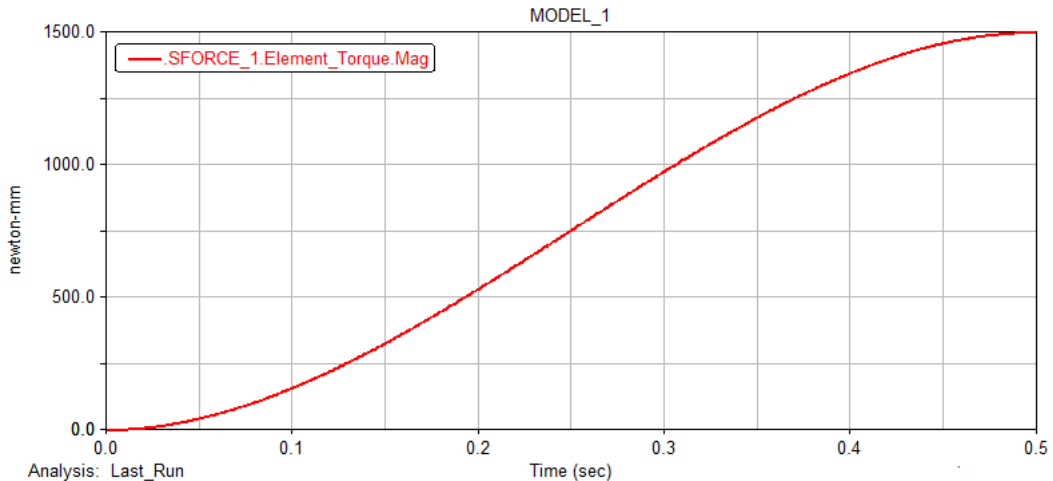


FIGURE 2.29: Input Torque characteristics

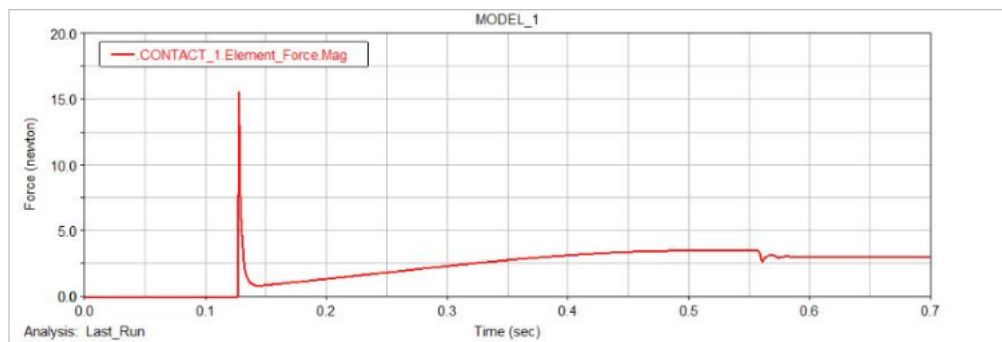


FIGURE 2.30: Contact force on first phalanx while grasping a sphere

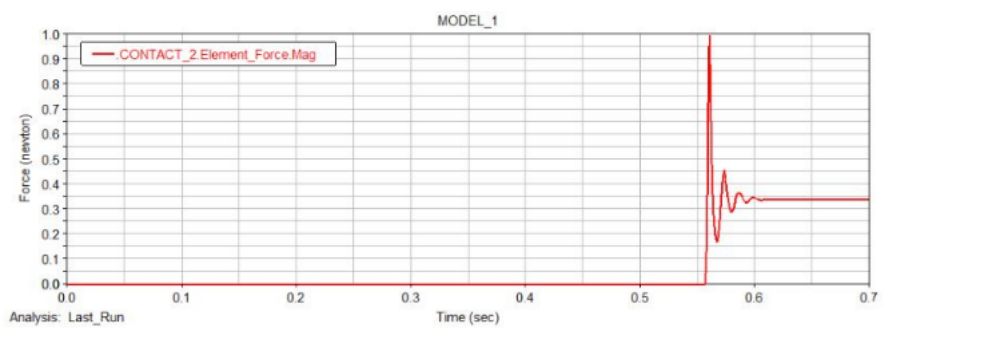


FIGURE 2.31: Contact force on second phalanx while grasping a sphere

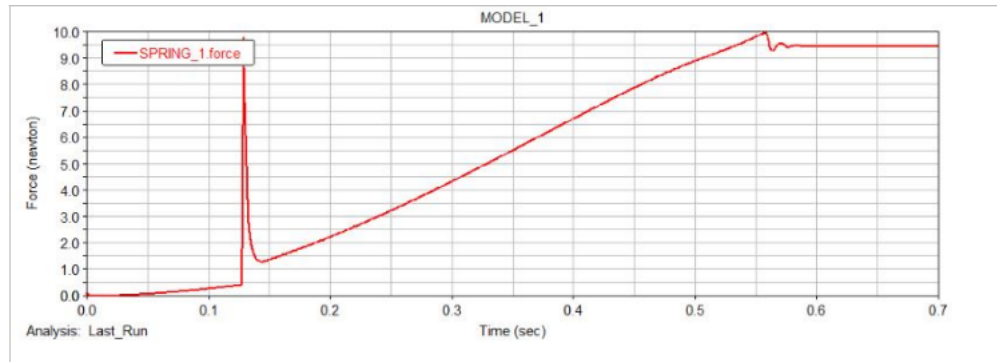


FIGURE 2.32: Extension Spring force while grasping the sphere

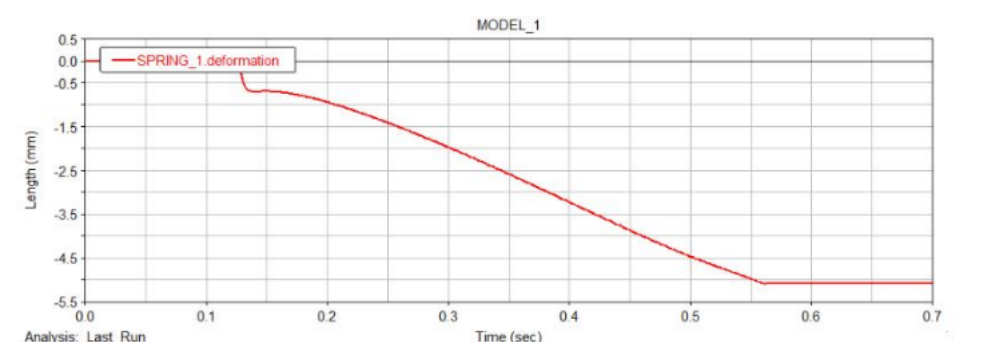


FIGURE 2.33: Spring deformation while grasping the sphere

2.3 Part drawings

Refer Appendix A

2.4 Bill of Material

The Bill of Material for the gripper is given in Appendix B , It includes the list of gripper elements with quantity, cost and source information needed to estimate the overall cost of the gripper prototype.

Chapter 3

Fabrication

In this chapter, we have discussed the employed manufacturing techniques used for manufacturing the gripper. As discussed in Chapter 1, in order to minimize the cost of manufacturing and present a product that is both cost efficient and feasible, we have employed the rapid prototyping technique (Additive manufacturing). In the present work, to further reduce the cost involved, we have utilized the available resources from STEP Lab (on campus facility)

3.1 Introduction

Rapid Prototyping (RP) is defined as a group of techniques used to quickly fabricate a scale model of a part or assembly using three-dimensional computer-aided design (CAD) data. Stereolithography is commonly considered to be the first RP technique which was developed by 3D Systems of Valencia, CA, USA. The company was founded in 1986, and since then, a number of different RP techniques have become available. Rapid Prototyping has also been referred to as solid free-form manufacturing, computer automated manufacturing, and layered manufacturing. Rapid Prototyping is commonly used for vehicles for visualization. In addition, Rapid Prototyping models can be used for testing, such as when an aerofoil shape is put into a wind tunnel. Rapid Prototyping models can be used to create male models for toolings, such as silicone rubber moulds and investment casts. In some cases, the Rapid Prototyped part can be the final part, but typically the Rapid Prototyping material is not strong or accurate enough. When the material to be used is suitable, highly convoluted shapes (including parts nested within parts) can be produced because of the nature of Rapid Prototyping.

There is a multitude of experimental Rapid Prototyping methodologies either in development or used by small groups of individuals. Some Rapid Prototyping techniques that are currently commercially available, includes Stereolithography (SLA), Selective Laser Sintering (SLS), Laminated Object Manufacturing (LOM), Fused Deposition Modelling (FDM), Solid Ground Curing (SGC), and Ink Jet printing techniques. The reasons for using Rapid Prototyping are given below

- To reduce wastage of material, instead of machining a component.
- To decrease development time.
- To minimize sustaining engineering changes.
- To extend product lifetime by adding necessary features and eliminating redundant features early in the design.

Rapid Prototyping decreases development time by allowing corrections to a product to be made early in the process. By giving engineering, manufacturing, marketing, and purchasing a look at the product early in the design process, mistakes can be corrected and changes can be made while they are still inexpensive. The trends in manufacturing industries continue to emphasize the following:

- Increasing the number of variants of products.

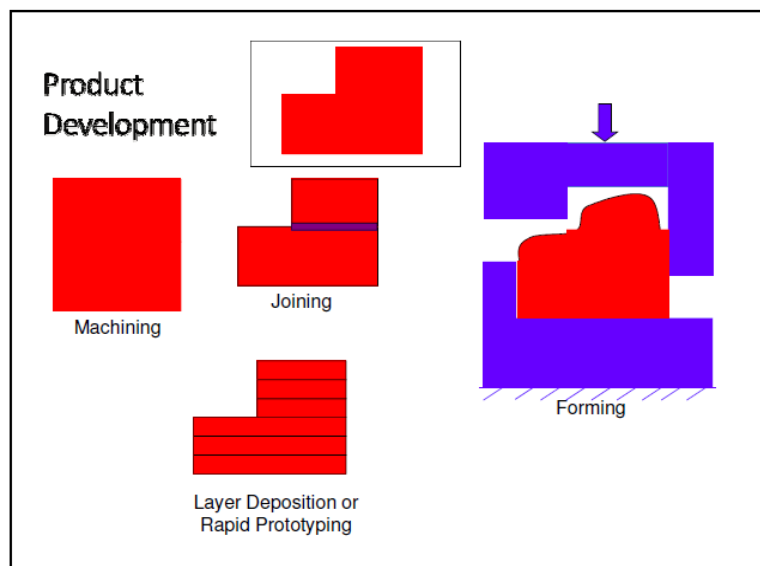


FIGURE 3.1: difference between the various methods of manufacturing a component

- Increasing product complexity.
- Decreasing product lifetime before obsolescence.
- Decreasing the delivery time.

Rapid Prototyping improves product development by enabling better communication in a concurrent engineering environment.

3.2 Methodology of Rapid Prototyping

The basic methodology for all current rapid prototyping techniques can be summarized as follows:

- A CAD model is constructed, then converted to STL format. The resolution can be set to minimize stair stepping.
- The rapid prototyping machine processes the .stl file by creating sliced layers of the model.
- The first layer of the physical model is created. The model is then lowered by the thickness of the next layer, and the process is repeated until the completion of the model.
- The model and any supports are removed. The surface of the model is then finished and cleaned.

3.2.1 Fused Deposition modeling

This is the technique which is nowadays very commonly used in manufacturing various components using rapid prototyping. This technique is used for the fabrication of our project. Almost all the components are fabricated using this technique.

Stratasys of Eden Prairie, MN makes Fused Deposition Modelling (FDM) machines. The FDM process was developed by Scott Crump in 1988. rapid prototyping The machines range from fast concept modellers to slower, high-precision machines. The materials include polyester, ABS, elastomers, and investment casting wax. In fact, the term ‘FDM’ is the trademark of Stratasys.

Alternatively, the 3D printers that are based on this technology are also called as Fused Filament Fabrication (FFF), Plastic Jet Printing (PJP) or material extruding printers, which is the generic name for these 3D printers.

The 3D printers that work on FDM technology consist of the printer platform, a nozzle (also called as printer head) and the raw material in the form of a filament. The printer

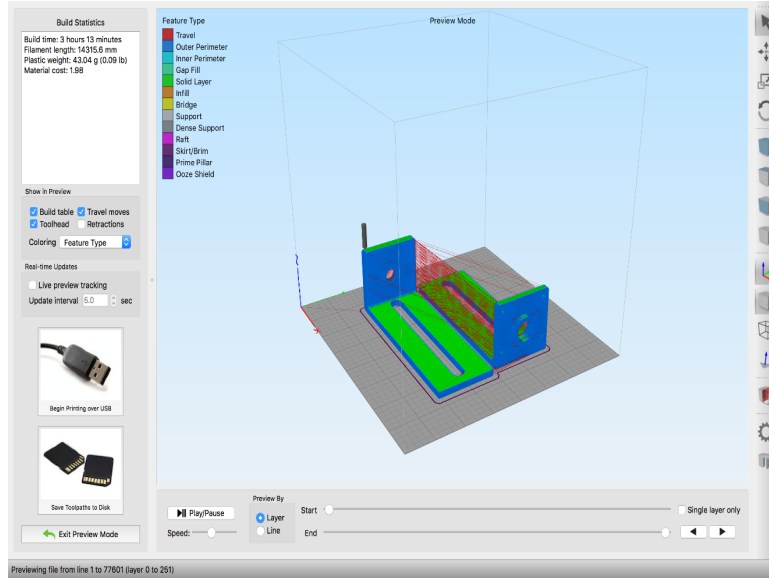


FIGURE 3.2: A .stl file being read on simplify 3d

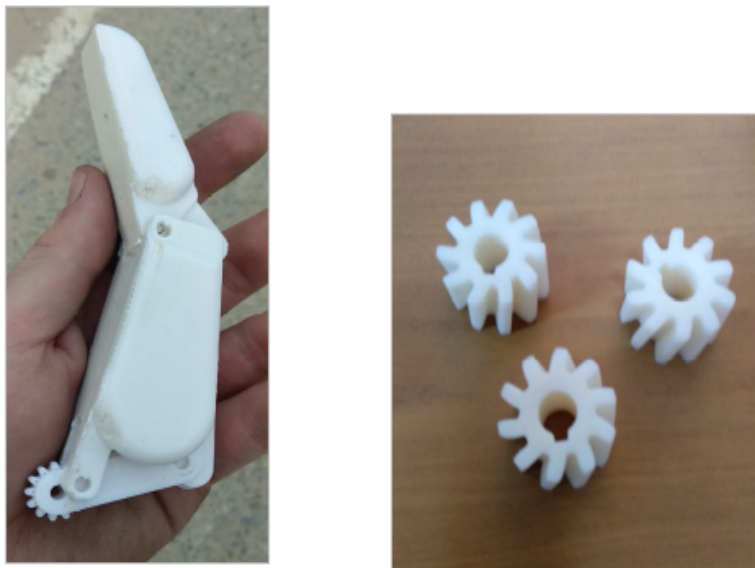


FIGURE 3.3: Components fabricated using FDM

platform or the bed is typically made of some metal, ceramic or glass and each successive layer is deposited on this platform.

The Nozzle / Printer Head

The nozzle of FDM printers is attached to a mechanical frame which uses belt and lead screw systems to move it. The entire extrusion assembly is allowed to move in X, Y and Z dimensions by a motorized system. A fourth motor called as the stepper motor is used to advance the thermoplastic material into the nozzle. All the movements of the head and the filament is controlled by a computer.

3.2.2 Raw material

The raw material is typically production grade thermoplastics, though sometimes metal is used as well. The thermoplastic material is capable of being repeatedly melted when exposed to heat and re-solidified when the heat is withdrawn. The thermoplastic filament or metal wire is wound as a coil on a mounted spool. It is then fed through the printer nozzle. The better class of 3D FDM printers allows the temperature of the nozzle to be maintained just close to the glass transition temperature of the material being extruded. This allows the material to be extruded in a semi-liquid state, but return to solid state immediately. This results in a better dimensional accuracy. In principle, any thermoplastic



FIGURE 3.4: Nozzle head of an FDM machine

can be used as raw material for FDM printers. Commercially, a few of the popular choices of raw material include nylon, Acrylonitrile Butadiene Styrene (ABS) and its variations, polycarbonates, poly-lactic acid, polystyrene and thermoplastic urethane. MED610, a raw material that Stratasys provides is bio-compatible. Their ULTEM material too is certified by the aerospace industry.

3.2.3 The FDM 3D Printing Process

When the FDM printer begins printing, the raw material is extruded as a thin filament through the heated nozzle. It is deposited at the bottom of the printer platform, where it solidifies. The next layer that is extruded fuses with the layer below, building the object from the bottom up layer by layer.

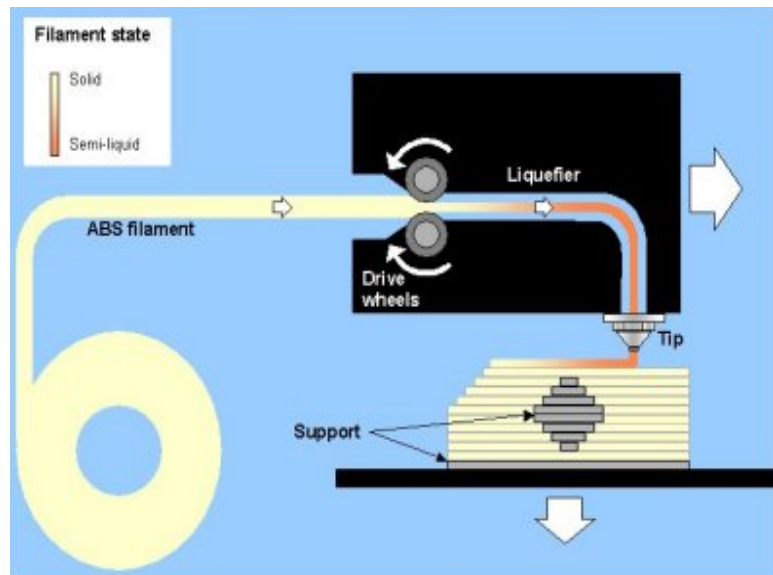


FIGURE 3.5: FDM 3D printing process.

Most FDM printers first print the outer edges, the interior edges next and lastly the interior of the layer as either a solid layer or as a fill in matrix.

In some objects / models, there are fragile ‘overhangs’ that will droop unless they are given some support. FDM printers incorporate a mechanism whereby these support structures (called struts) are printed along with the object. They are later removed once the build is complete. These struts are usually of the same material as the object. Some printers have a second extruder to specifically deposit soluble thermoplastic struts when there is a need to prevent the overhangs from drooping. These struts may be of a different composition

than the thermoplastic used for the 3D model. They are later dissolved by an appropriate solvent.

3.2.4 Accuracy of 3D FDM Printers

As discussed earlier that a 3D printer works by depositing raw material layer by layer along the X, Y and Z axis. The accuracy of the 3D printer therefore depends upon the minimum distance the nozzle can travel vertically (the Z axis). Minimum the distance it can move, more the points along the sinusoid that it can capture, and better the accuracy. For Stratasys 3D printers, which are the pioneers of the FDM printers, the current best possible dimensional accuracy is about 0.127 mm. Of course, the choice of raw material too plays an important part in achieving dimensional stability. It should also be remembered that the accuracy comes at the cost of printing time required. A few advantages of FDM



FIGURE 3.6: Stratasys uprint an FDM machine.

3D printers include:

- A wide range of FDM printers are available in the market today
- the raw material is inexpensive, durable and maintains dimensional integrity
- there is a wide choice of raw material
- they are affordable
- low turnaround time

One disadvantage is that if the desired level of accuracy is extremely high, then the FDM printers may be found wanting. FDM 3D Printers find application in:

- creating prototypes for Fit, Form and Function testing
- rapid tooling patterns and mould inserts
- creating and testing any parts that work under thermal loads
- production of precise and complex end-use parts e.g. jigs and fixtures

Sectors that use FDM 3D Printers include: Automotive, Aerospace, Manufacturing, Industrial, Medical, Architecture, Consumer Goods, Fashion and Education and Research

Overall, FDM 3D printers give a very high value for money and are very popular in India and other countries.

Chapter 4

Post-Fabrication analysis

Shrinkage is inherent in the injection molding process. Shrinkage occurs because the density of polymer varies from the processing temperature to the ambient temperature (see Specific volume (pvT diagram)). During injection molding, the variation in shrinkage both globally and through the cross section of a part creates internal stresses. These so-called residual stresses (see Residual stress) act on a part with effects similar to externally applied stresses. If the residual stresses induced during molding are high enough to overcome the structural integrity of the part, the part will warp upon ejection from the mold or crack with external service load.

4.1 Shrinkage

The shrinkage of molded plastic parts can be as much as 20 percent by volume, when measured at the processing temperature and the ambient temperature. Crystalline and semi-crystalline materials are particularly prone to thermal shrinkage; amorphous materials tend to shrink less. When crystalline materials are cooled below their transition temperature, the molecules arrange themselves in a more orderly way, forming crystallites. On the other hand, the microstructure of amorphous materials does not change with the phase change. This difference leads to crystalline and semi-crystalline materials having a greater difference in specific volume (ΔV) between their melt phase and solid (crystalline) phase. This is illustrated in Figure 4.1 below. We'd like to point out that the cooling rate also affects the fast-cooling pvT behavior of crystalline and semi-crystalline materials.

4.1.1 Cause of excessive shrinkage

Excessive shrinkage, beyond the acceptable level, can be caused by the following factors. The relationship of shrinkage to several processing parameters and part thickness is schematically plotted in Figure 4.2. Problems caused by part shrinkage:

- low injection pressure
- short pack-hold time or cooling time
- high melt temperature
- high mold temperature
- low holding pressure.

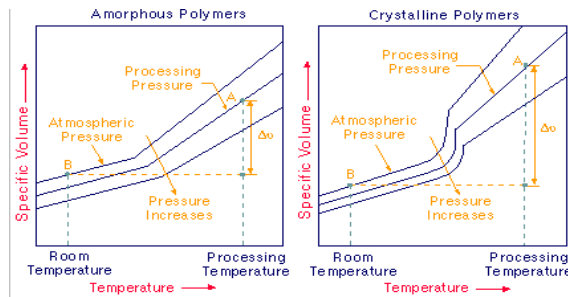


FIGURE 4.1: The pVT curves for amorphous and crystalline polymers and the specific volume variation (ΔV) between the processing state (point A) and the state at room temperature and atmospheric pressure (point B). Note that the specific volume decreases as the pressure increases.

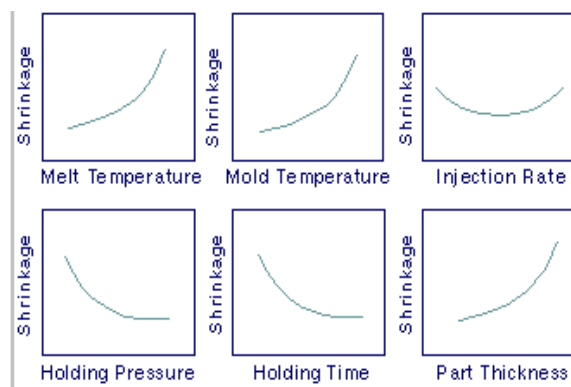


FIGURE 4.2: Processing and design parameters that affect part shrinkage.

4.1.2 Problems caused by part shrinkage

Uncompensated volumetric contraction leads to either sink marks or voids in the molding interior. Controlling part shrinkage is important in part, mold, and process designs, particularly in applications requiring tight tolerances. Shrinkage that leads to sink marks or voids can be reduced or eliminated by packing the cavity after filling. Also, the mold design should take shrinkage into account in order to conform to the part dimension. Part shrinkage predicted by C-MOLD offers a useful guideline for proper mold design.

4.2 Warpage

Warpage is a distortion where the surfaces of the molded part do not follow the intended shape of the design. Part warpage results from molded-in residual stresses, which, in turn, is caused by differential shrinkage of material in the molded part. If the shrinkage throughout the part is uniform, the molding will not deform or warp, it simply becomes smaller. However, achieving low and uniform shrinkage is a complicated task due to the presence and interaction of many factors such as molecular and fiber orientations, mold cooling, part and mold designs, and process conditions. Warpage in molded parts results from differential shrinkage. Variation in shrinkage can be caused by molecular and fiber orientation, temperature variations within the molded part, and by variable packing, such as over-packing at gates and under-packing at remote locations, or different pressure levels as material solidifies across the part thickness. These causes are described more fully below.

- Differences in filled and unfilled materials
- Non-uniform mold cooling across the part thickness or over the part
- Cooling rates that differ because of Part thickness variation
- Part geometry asymmetry or curvature

Differences in filled and unfilled materials

Differential shrinkage for filled and unfilled materials is shown in Figure 4.3 below. When shrinkage is differential and anisotropic across the part and part thickness, the internal stresses created can lead to part warpage.

- **Filled materials** For fiber-filled thermoplastics, reinforcing fibers inhibit shrinkage due to their smaller thermal contraction and higher modulus. Therefore, fiber-filled materials shrink less along the direction in which fibers align (typically the flow direction) compared to the shrinkage in the transverse direction. Similarly, particle-filled thermoplastics shrink much less than unfilled grades.
- **Unfilled materials** On the other hand, if an unfilled molded part contains high levels of molecular orientation, shrinkage is anisotropic because aligned chains shrink to a greater extent in the direction of orientation.
- **Liquid crystal polymers** For liquid crystal polymers (LCPs), the tightly ordered self-reinforcing structure tends to exhibit anisotropic shrinkage.

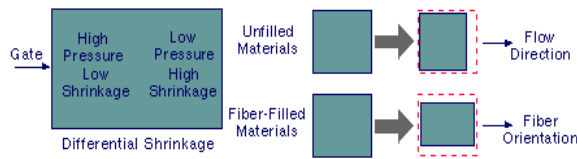


FIGURE 4.3: Differential shrinkage for both unfilled and filled materials.

Non-uniform mold cooling across the part thickness

Non-uniform cooling in the part and asymmetric cooling across the part thickness from the mold cavity and core can also induce differential shrinkage. The material cools and shrinks inconsistently from the mold wall to the center, causing warpage after ejection.

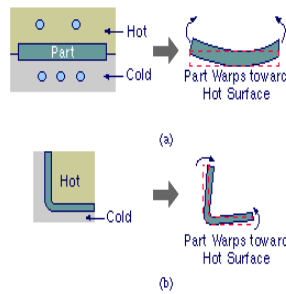


FIGURE 4.4: Part warpage due to (a) non-uniform cooling in the part, and (b) asymmetric cooling across the part thickness..

Part thickness variation

Shrinkage increases as the wall thickness increases. Differential shrinkage due to non-uniform wall thickness is a major cause of part warpage in unreinforced thermoplastics.

More specifically, different cooling rates and crystallization levels generally arise within parts with wall sections of varying thickness. This causes differential shrinkage, resulting in part warpage, as shown in Figure 4.5

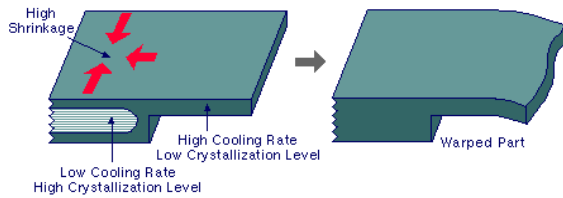


FIGURE 4.5: Larger volumetric shrinkage due to the high crystallization level in the slow cooling areas (e.g., the thick sections) leads to differential shrinkage and thus part warpage.

Part geometry asymmetry or curvature

Geometric asymmetry (e.g., a flat plate with a large number of ribs that are aligned in one direction or on one side of the part) will introduce non-uniform cooling and differential shrinkage that can lead to part warpage, as shown in Figure 4.6.

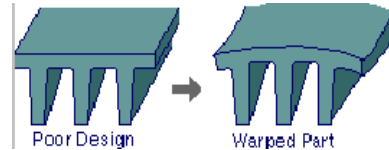


FIGURE 4.6: The poor cooling of the mold wall on the ribbed side causes a slower cooling of the material on that one side, which can lead to part warpage.

Chapter 5

Conclusion

This paper presents the design of an underactuated robotic end effector with a breakaway clutch mechanism. A novel application of a breakaway clutch mechanism using helical gears is presented. This mechanism provides independent movement of the fingers actuated by a single actuator. The end effector design model and its prototype are introduced and discussed in detail. It is shown that the the presented robotic end effector with one actuator meets the design objectives in terms of:

- simple mechanical structure of the end effector due to usage of a four-bar linkage system;
- a low cost due to usage of a single actuator, 3D printing prototyping technology and off-the-shelf components;
- relatively high payload comparable with currently available robotic end effectors.

Overall, the proposed end effector design can be potentially preferable in terms of cost to payload ratio. The 3D model of the gripper is created using Solidworks software and linear static force analysis is caried out to compute the Vonmisses stress and elemental displacement also the dynamic analysis is performed to validate the feasibility and performance of the gripper mechanism. This simple three finger gripper would serve as a suitable alternative to the unskilled labor and would benefit the small scale warehouses by fulfilling their requirements and to maximize the productivity. Future work includes design and implementation of proposed end effector prototype with embedded sensing elements such as tactile sensors for force feedback capabilities and depth camera for object recognition to perform autonomous grasping performance. There are ongoing attempts

to improve grippers in two-fold: performance and flexibility. Performance indicates accuracy, speed, readability, gripping strength, robustness, and flexibility denotes variety of objects that can be grasped. Most of the challenge in this aspect is whether objects are known/unknown. When one is dealing with unknown objects, the focus is to employ flexible grippers, while in grasping known objects, the focus is on the increasing the performance. Achieving flexibility and performance simultaneously still remains challenging because increasing performance usually results in decreasing flexibility.

Chapter 6

Appendix A

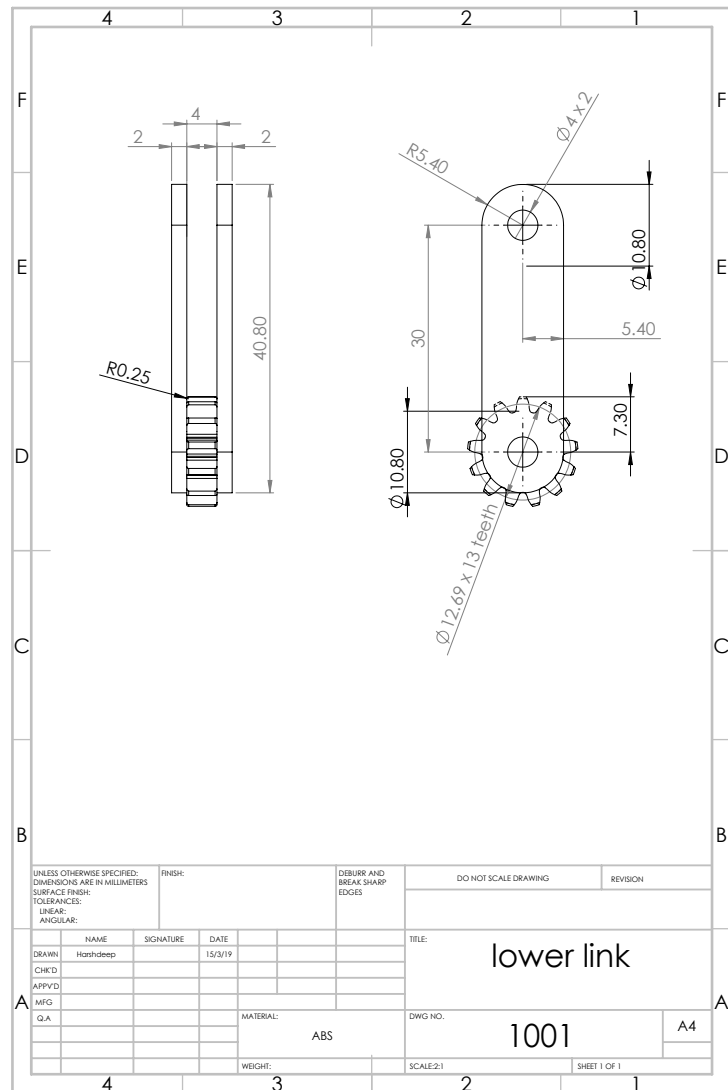


FIGURE 6.1: Lower link

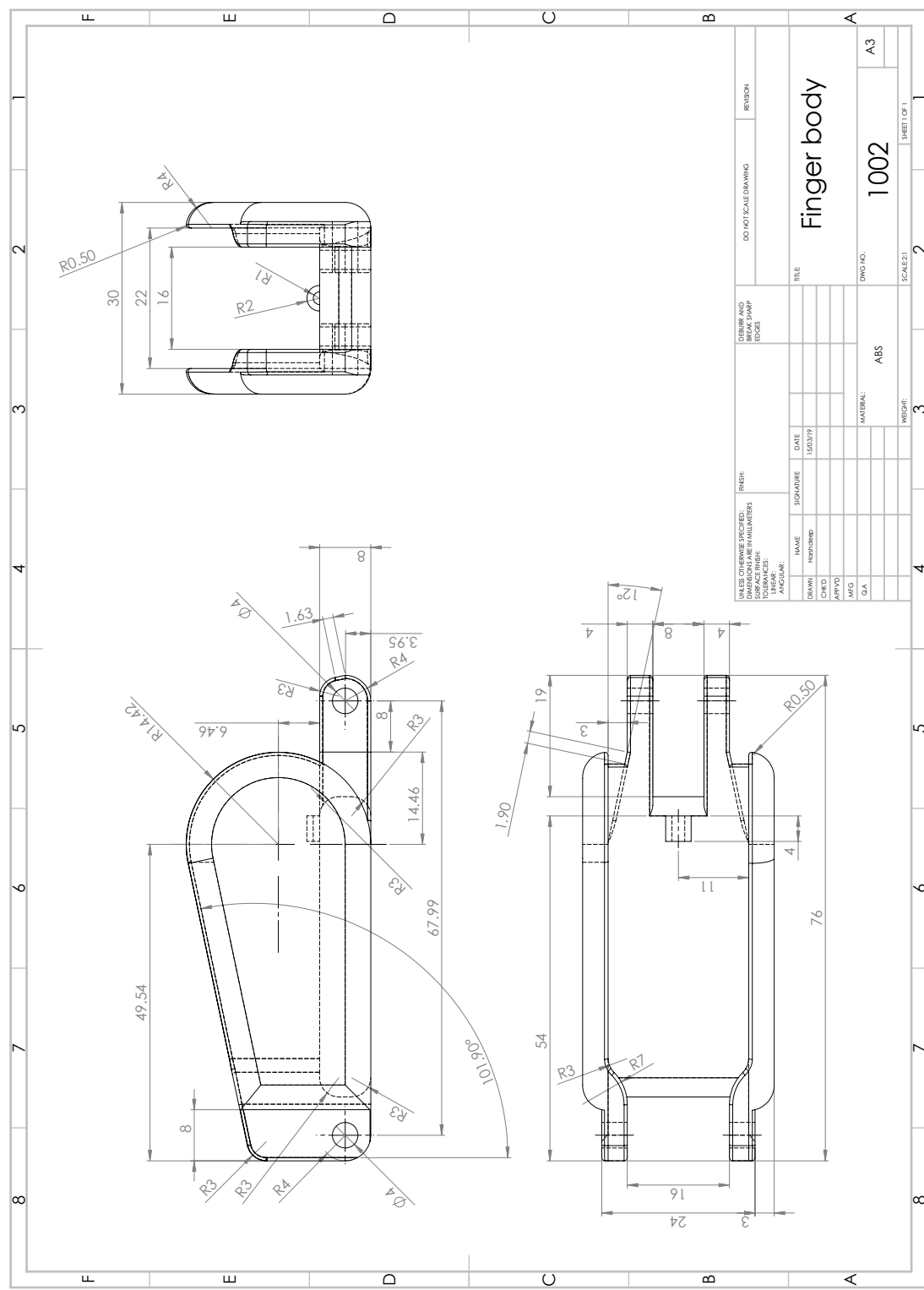


FIGURE 6.2: Finger body

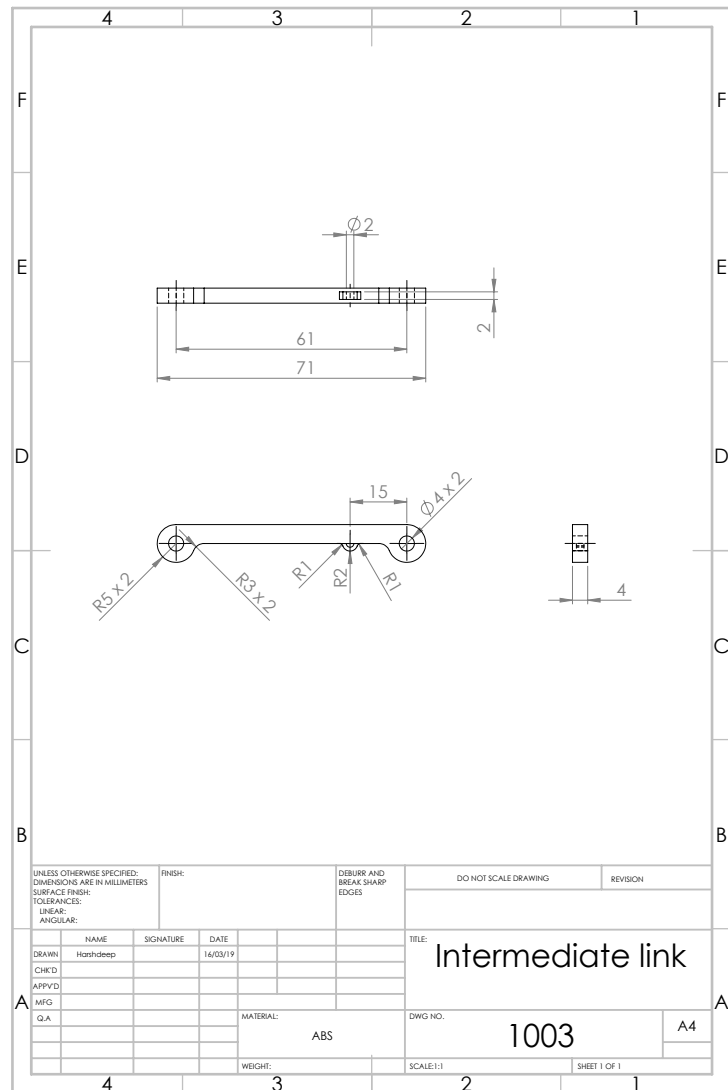


FIGURE 6.3: Intermediate link

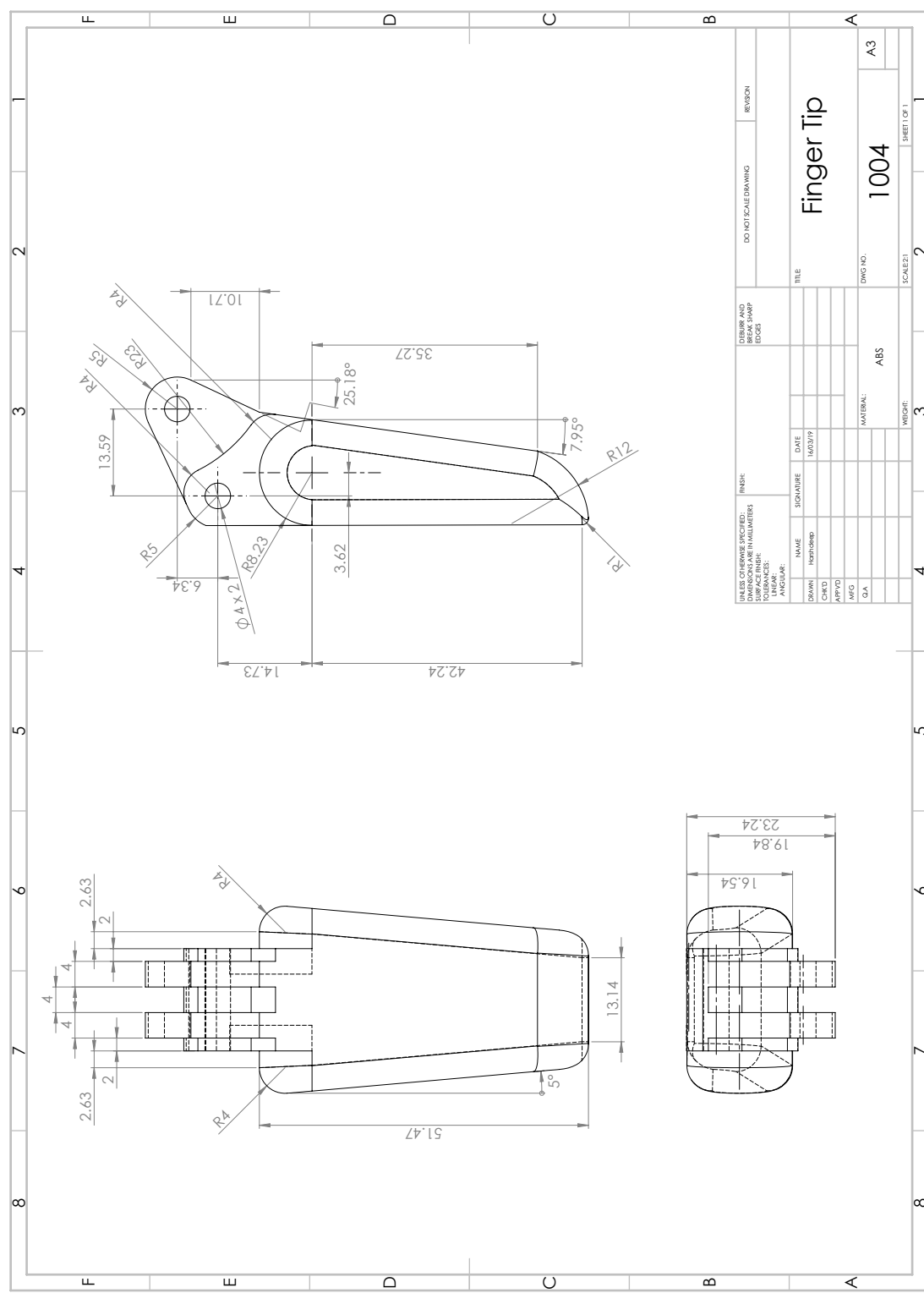


FIGURE 6.4: Finger tip

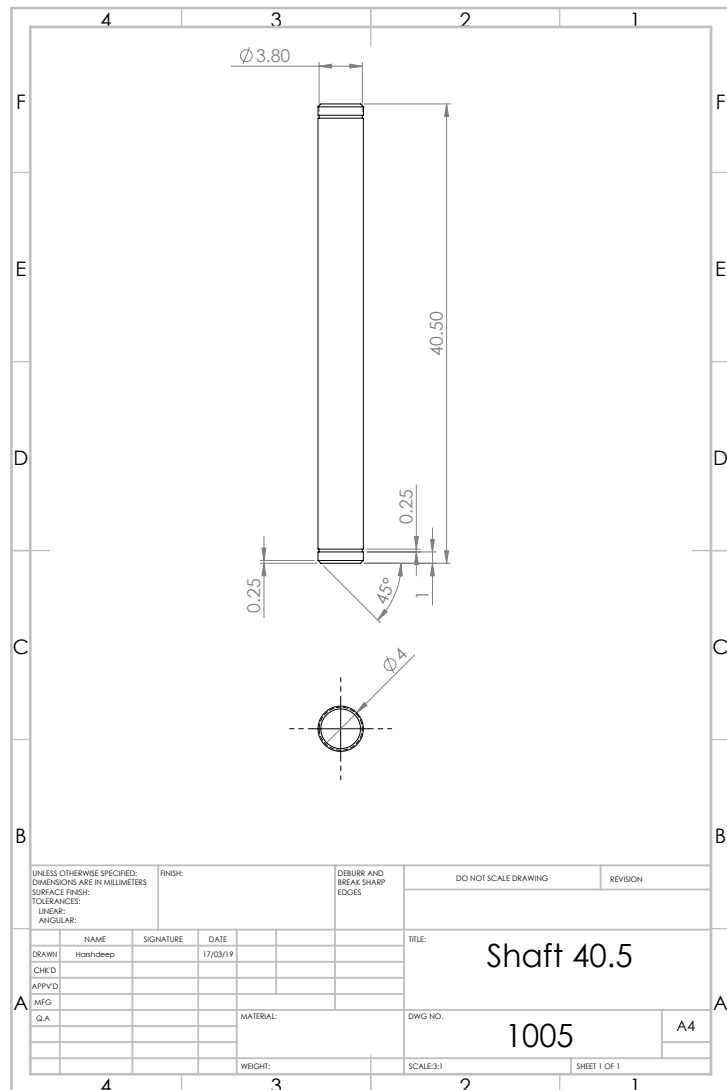


FIGURE 6.5: Shaft 40.5

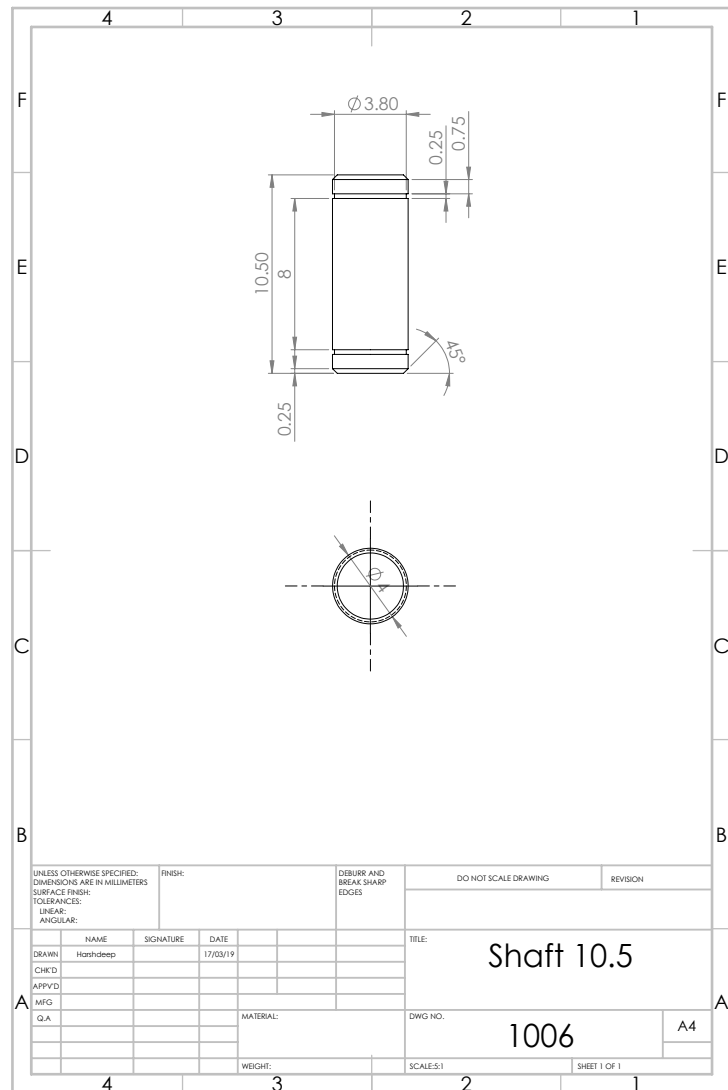


FIGURE 6.6: Shaft 10.5

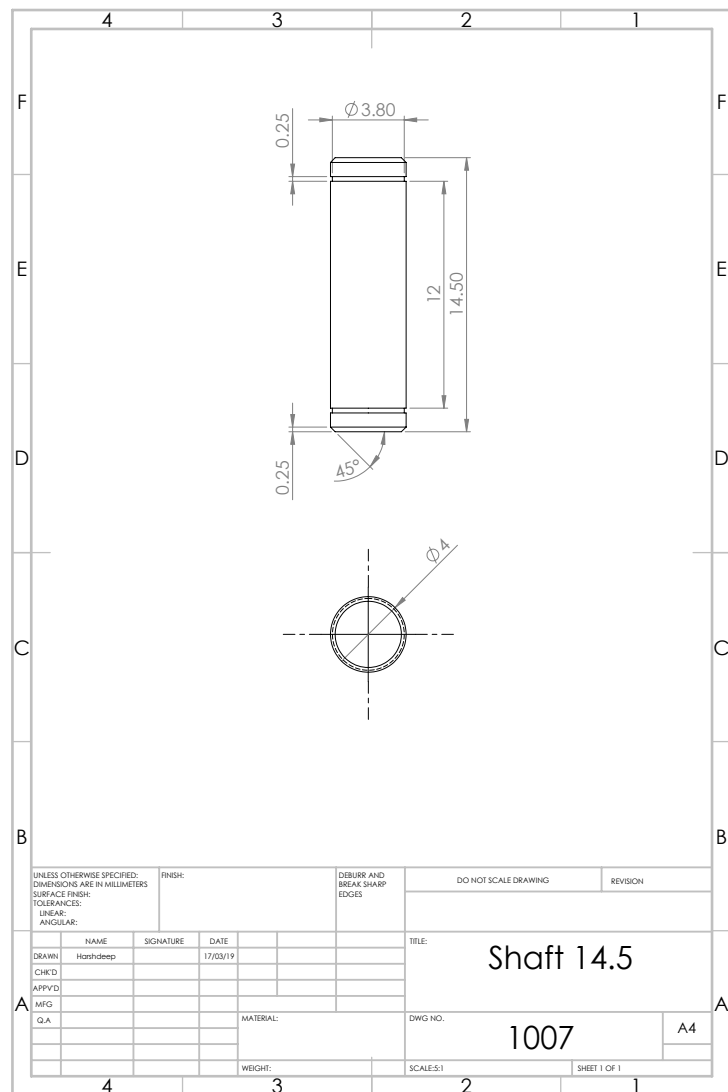


FIGURE 6.7: Shaft 14.5

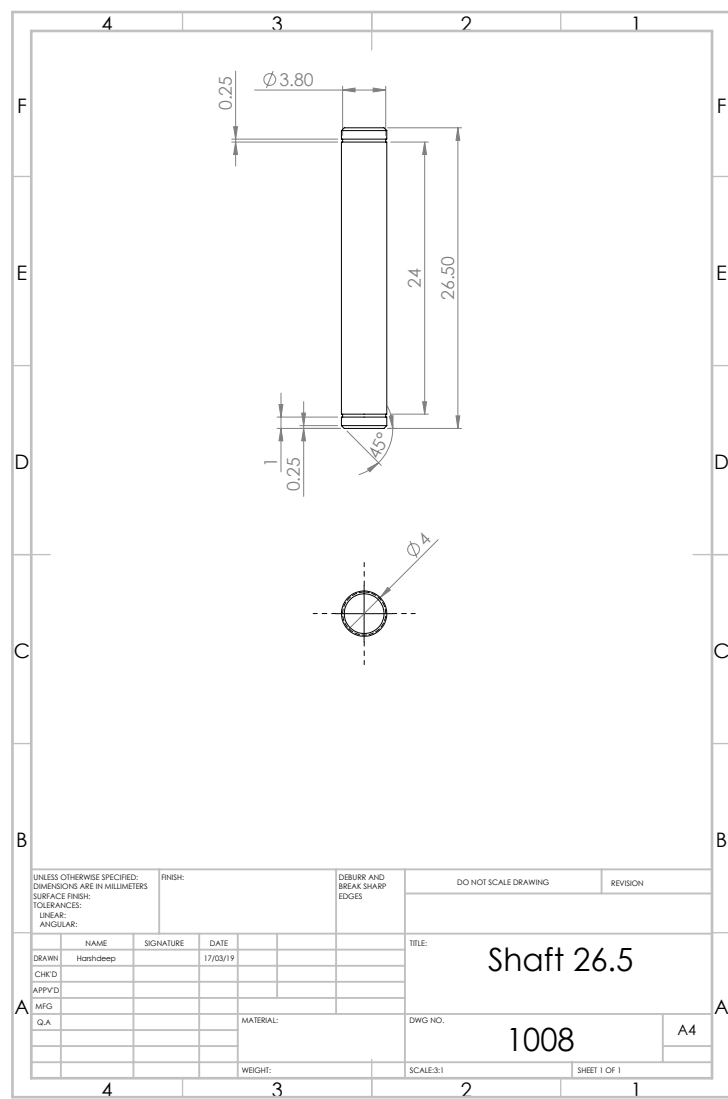


FIGURE 6.8: Shaft 26.5

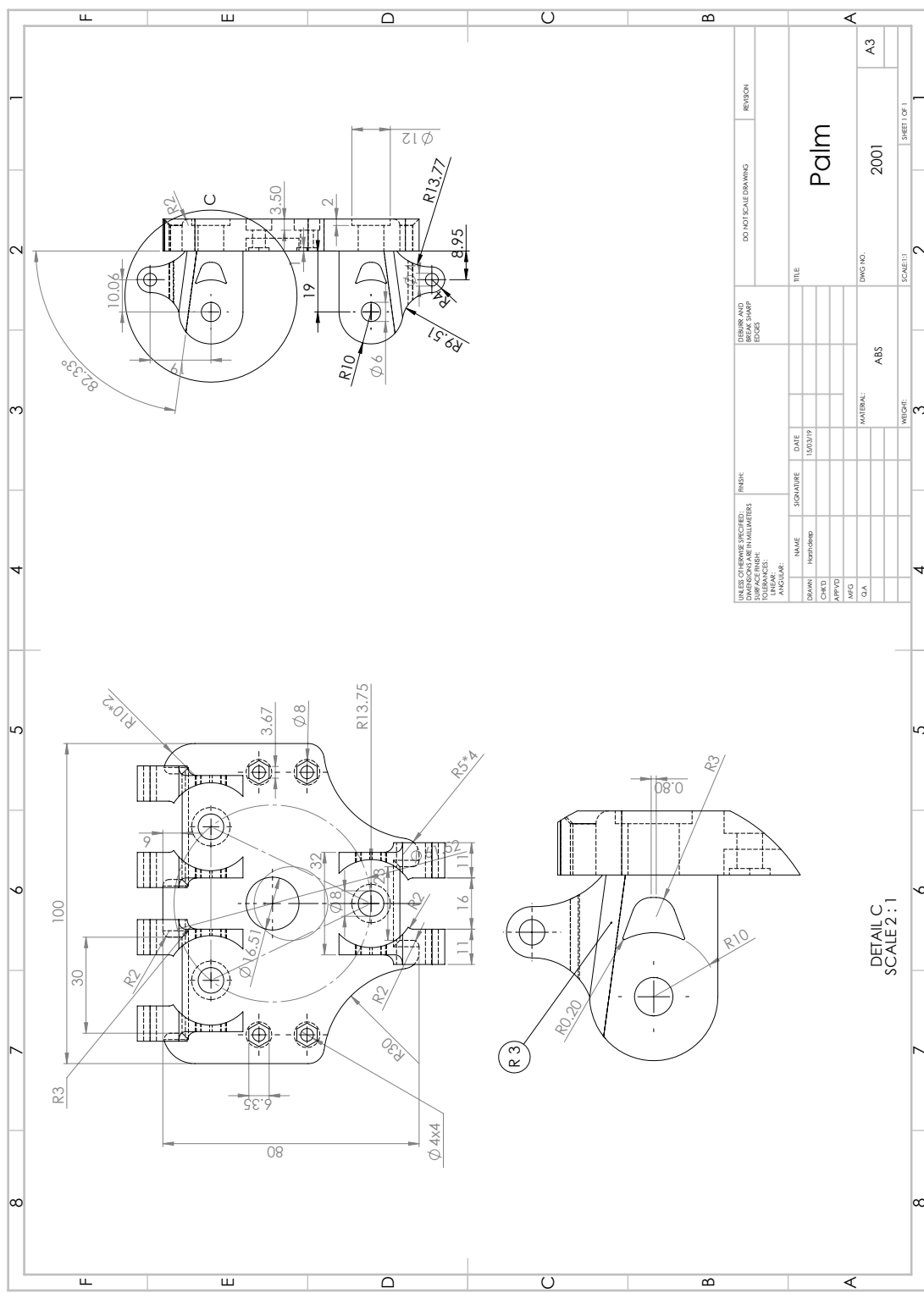


FIGURE 6.9: Palm

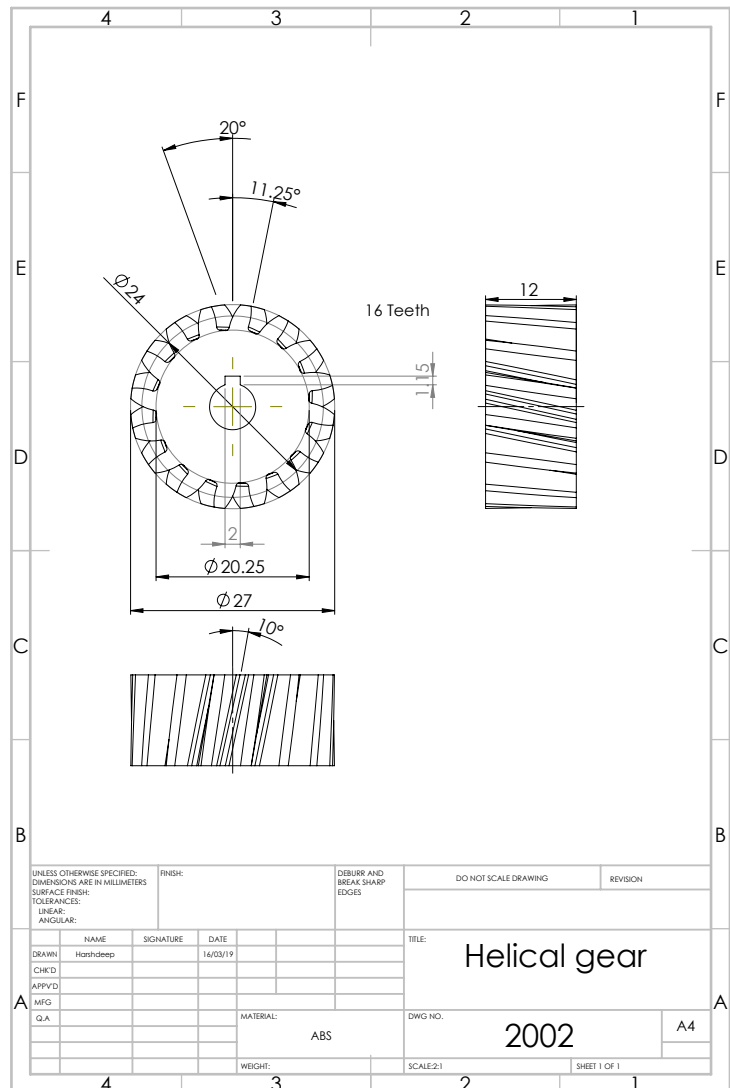


FIGURE 6.10: Helical gear

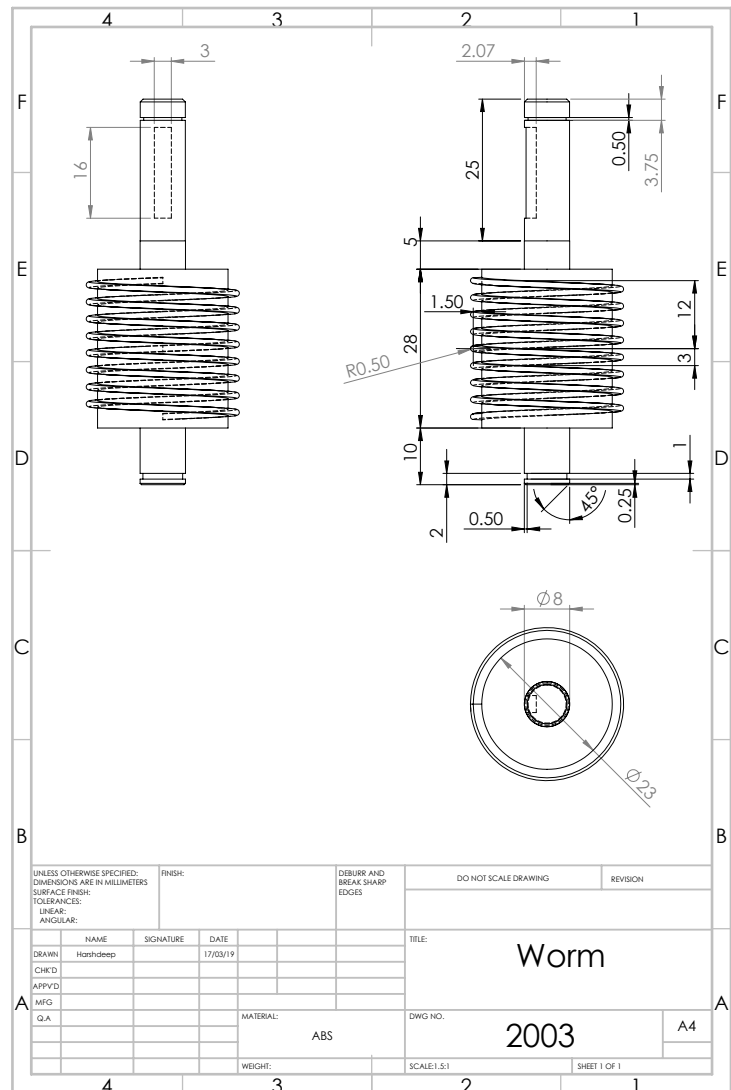


FIGURE 6.11: Worm

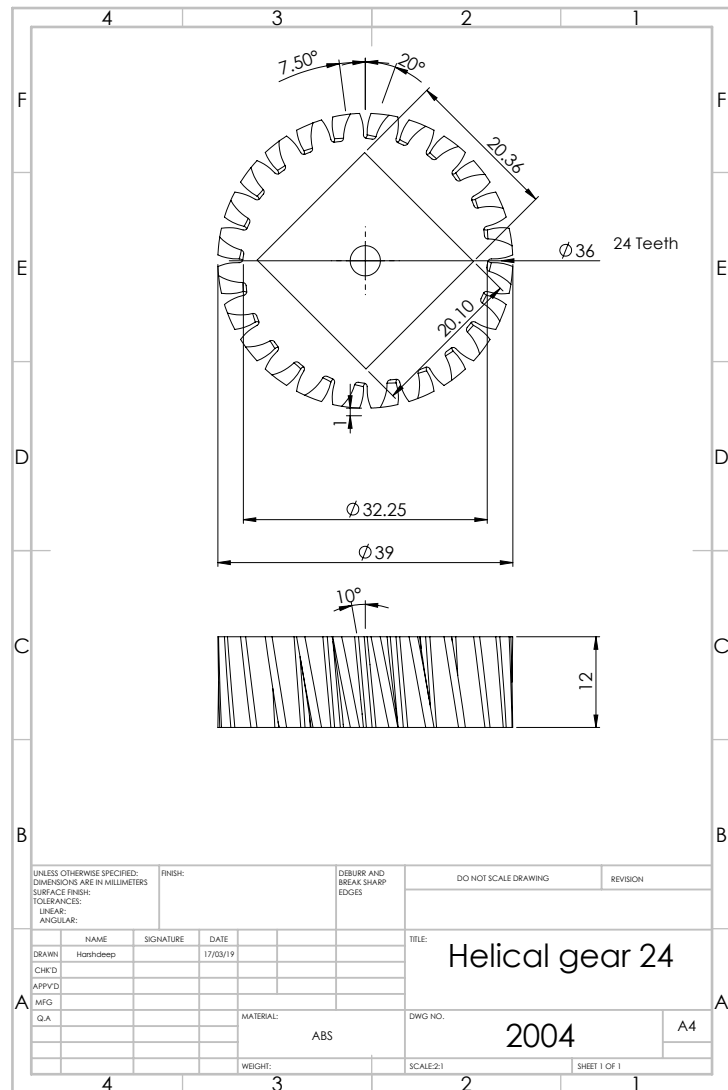


FIGURE 6.12: Helical gear 24

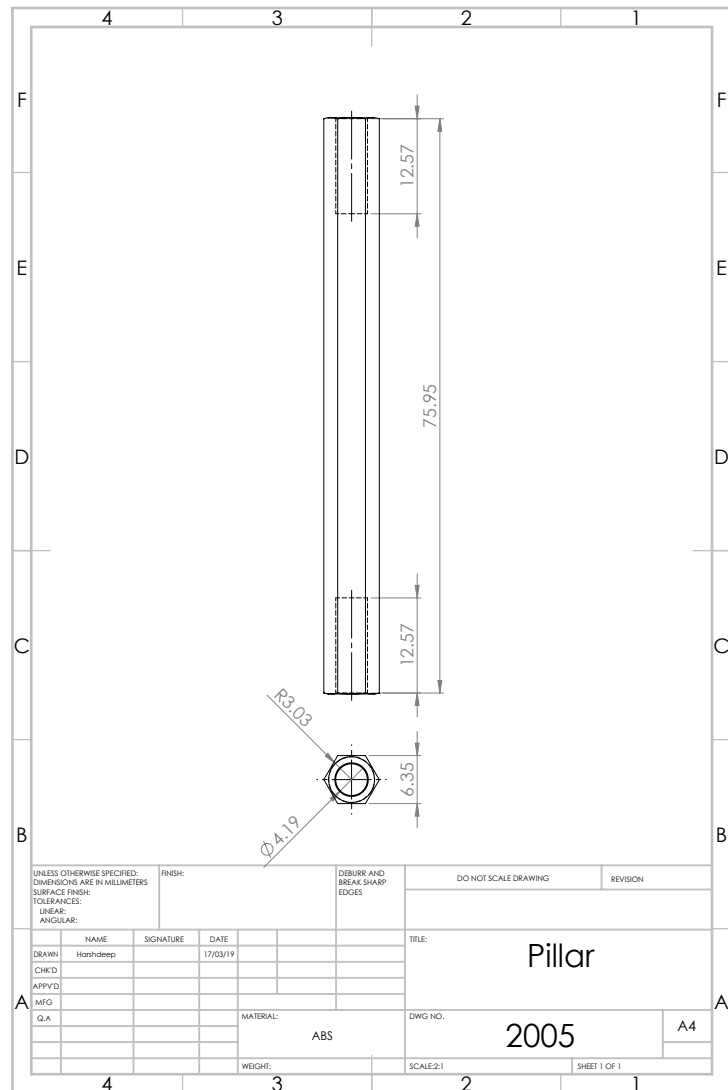


FIGURE 6.13: Pillar

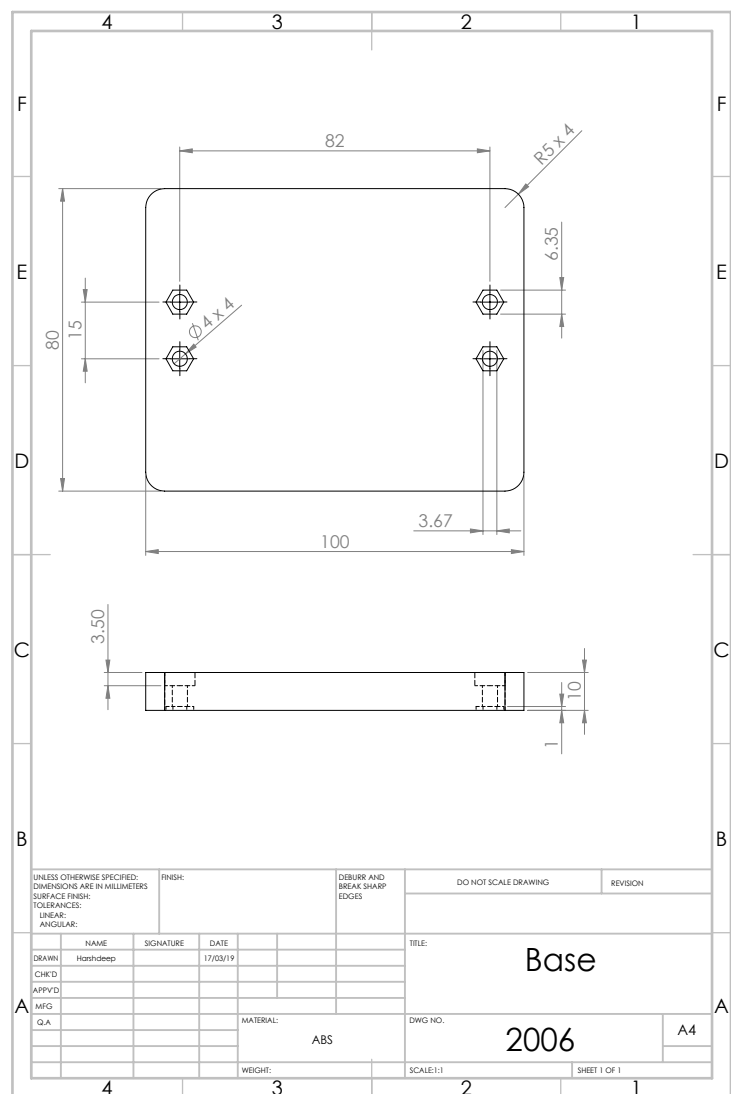


FIGURE 6.14: Base

Chapter 7

Appendix B

S.no	PART NUMBER	DESCRIPTION	QTY.	Material	Drawing	weight(grams) 100% infl	Source	Cost	1.25 g/cm ³
1	Palm		1	ABS	Y	80	3D Printing Thapar	-	1100/kg
2	lower link		3	ABS	Y	1.456	3D Printing Thapar	-	1100/kg
3	finger body		3	ABS	Y	14.924	3D Printing Thapar	-	1240/kg
4	Pin 3	Φ4x40.5	3	steel	Y	Workshop Thapar	-		
5	upper link		3	ABS	Y	1.148	3D Printing Thapar	-	1.05 g/cm ³
6	phalanx_2		3	ABS	Y	14	3D Printing Thapar	-	1573/kg
7	Pin 4	Φ4x10.5	3	steel	Y	Workshop Thapar	-		
8	Retaining ring	6 mm	3	steel		Hardware Shop	50	Rapid3D	1300/kg
8	Retaining ring	4mm	24	Steel		Hardware Shop	200		900/kg
9	Pin 5	Φ4x14.5	3	steel	Y	Workshop Thapar	-		
10	Pin 2	Φ4x26.5	3	steel	Y	Workshop Thapar	-		
11	Worm		3	ABS	Y	11.326	3D Printing Thapar	-	1.15 g/cm ³
12	Helical gear	10 teeth	3	ABS	Y	13.552	3D Printing Thapar	-	3000/kg
13	Helical gear	18 teeth	1	ABS	Y	3.003	3D Printing Thapar	-	3014.85/kg
14	Actuator	2.5 Km 55 RPM	1			Tolex Springs Maharashtra	8000	Reiddx Technologies	2950/kg
15	Spring	2N/mm Stiffness	3			Tolex Springs Maharashtra	1100	PC	1.20 g/cm ³
16	Spring	1N/mm	3			Robokits india	900	Hatchbox	4300/kg
17	Filament ABS		1 spool				2600	Fab.to.lab	3150/kg
18	Force sensors		3				2000	3D Sculpto	3000/kg
19	Arduino Uno		1				1500		
Total									16300

FIGURE 7.1: Bill of Material

Chapter 8

References

1. S. Jacobsen, E. Iversen, D. Knutti, R. Johnson, and K. Biggers, “Design of the Utah/M.I.T. Dextrous Hand,” Proc. of the 1986 IEEE Int. Conf. on Robotics and Automation, pp. 1520-1532, 1986.
2. M. Baril, T. Laliberte, C. Gosselin, and F. Routhier, “On the Design of a Mechanically Programmable Underactuated Anthro- pomorphic Prosthetic Gripper,” ASME J. of Mechanical Design, Vol.135, No.12, p. 121008, 2013.
3. T. Laliberte, L. Birglen, and C. Gosselin, “Underactuation in robotic grasping hands, Machine Intelligence and Robotic Control,” Vol.4, No.3, pp. 1-11, 2002.
4. Y. Ando, “Microgripper,” J. of Robotics and Mechatronics, Vol.2, No.3, pp. 214-216, 1990.
5. F. Chen, K. Sekiyama, B. Sun, P. Di, J. Huang, H. Sasaki, and T. Fukuda, “Design and Application of an Intelligent Robotic Grip- per for Accurate and Tolerant Electronic Connector Mating,” J. of Robotics and Mechatronics, Vol.24, No.3, pp. 441-451, 2012.
6. S. Bachche and K. Oka, “Design, Modeling and Performance Test- ing of End- Effector for Sweet Pepper Harvesting Robot Hand,” J. of Robotics and Mechatronics,

- Vol.25, No.4, pp. 705-717, 2013.
7. G. Figliolini and M. Sorli, "Open-Loop Force Control of a Three-Finger Gripper Through PWM Modulated Pneumatic Digital Valves," *J. of Robotics and Mechatronics*, Vol.12, No.4, pp. 480- 493, 2000.
 8. A. Namiki, Y. Imai, M. Kaneko, and M. Ishikawa, "Development of a High-Speed Multifingered Hand System," *Proc. of the 2003 IEEE/RSJ Int. Conf. on Intelligent Robots and Systems*, pp. 2666- 2671, 2004.
 9. W. Townsend, "The Barret Hand grasper - programmably flexible part handling and assembly," *Industrial Robot*, Vol.27, pp. 181-188, 2000.
 10. L. U. Odhner et al., "A compliant, underactuated hand for robust manipulation," *Int. J. of Robotics Research*, Vol.33, No.5, pp. 736- 752, 2014.
 11. S. J. Bartholet, "Reconfigurable end effector," U.S. Patent No:5108140, 1992.
 12. C. Gosselin, "Adaptive Robotic Mechanical Systems: A Design Paradigm," *ASME J. of Mechanical Design*, Vol.128, No.1, pp. 192- 198, 2005.
 13. C. Beyer, "Strategic implications of current trends in additive manufacturing," *ASME J. of Manufacturing Science and Engineering*, Vol.136, No.6, p. 064701, 2014.
 14. R. R. Ma, L. U. Odhner, and A. M. Dollar, "A modular, open-source 3D printed underactuated hand," *Proc. of the 2013 IEEE Int. Conf. on Robotics and Automation*, pp. 2737-2743, 2013.
 15. Z. Kappassov, Y. Khassanov, A. Saudabayev, A. Shintemirov, and H. A. Varol, "Semi-anthropomorphic 3D printed multigrasp hand for industrial and service robots," *Proc. of the 2013 IEEE Int. Conf. on Mechatronics and Automation*, pp. 1697-1702, 2013.